Intrinsic Kinetics of Lower Alcohols: C_2, C_3 Dehydration over Lewis Acidic Ordered Mesoporous Silicate: Zr-KIT-6

By

Qing Pan

Submitted to the graduate degree program in Chemical & Petroleum Engineering and the Graduate Faculty of the University of Kansas in partial fulfillment of the requirements for the degree of Master of Science.

_____

Chairperson: Dr. Bala Subramaniam

_____

Dr. Raghunath V. Chaudhari

_____

Dr. Anand Ramanathan

Date Defended: 08/27/2013

The Thesis Committee for Qing Pan

certifies that this is the approved version of the following thesis:

Intrinsic Kinetics of Lower Alcohols: C_2, C_3 Dehydration over Lewis Acidic Ordered Mesoporous Silicate: Zr-KIT-6

_____

Chairperson: Dr. Bala Subramaniam

Date approved: 09/06/2013

ABSTRACT

KIT-6 materials are large pore cubic Ia3d mesoporous silicate, with tunable pore size (4–12 nm) and pore wall thickness (4–6 nm). The three-dimensional structure of KIT-6 provides more mass transfer channels within the pore structure and also reduces the propensity for pore blockage. With the incorporation of zirconium into KIT-6 structure, the materials displayed mild Lewis acidity exclusively. These characteristics allow Zr-KIT-6 to be a promising catalyst for alcohol dehydration to olefins. Therefore, the emerging biomass-based renewable chemicals industry will particularly benefit from the availability of such catalysts for dehydration of long-chain alcohols from biomass based feedstock.

In this study, the dehydration of short-chain alcohols, including isopropanol (IPA) and ethanol (EtOH), were carried out over three Zr-MIT-6 samples with different Si/Zr ratios ranging from 20 to 100. In the temperature range of 180-300 °C, the Zr-KIT-6 materials were shown to be highly active for of IPA dehydration to propylene (selectivity >98.5%). While, ethylene formed with the selectivity of 70%-80% when dehydrating EtOH at 300-380 °C range. 30 h continuous run revealed slight catalyst deactivation for IPA dehydration; and the catalyst started to deactivate after 60 h for EtOH dehydration. Kinetic models were established for both of these two reactions. The activation energy for IPA and EtOH dehydration, estimated from intrinsic rate constants normalized with respect to the Lewis acid sites, were approximately 48.9 ± 0.5 kJ/mol and 79.5 ± 0.7 kJ/mol, respectively, which are found to be lower than or comparative with most other

Brønsted or Lewis acidic heterogeneous catalysts reported in the literature for such reactions. This clearly shows that the Zr-KIT-6 materials are a superior and promising class of highly active, selective and durable alcohol dehydration catalysts. Although, IPA and EtOH are short-chain alcohols, establishing such activity is key to their potential use as solid acid catalysts for even bulkier substrates.

DEDICATED TO

My family

ACKNOWLEDGEMENTS

I would not have been able to finish this thesis without the support, guidance, help, and encouragement from all the kind people around me, to only some of whom it is possible to give particular mention here.

First of all, I would like to express my deepest gratitude to my advisor, Professor Bala Subramaniam, not only for his professional guidance and support throughout my graduate study, but also for his indefatigable patience and encouragement whenever I had a rough time in the research. His wisdom, knowledge and commitment to the highest standards always inspired and motivated me.

I would also like to thank my committee members, Professor Raghunath V. Chaudhari and Dr. Anand Ramanathan, for their valuable instructions and feedback in my research and thesis writing. In particular, I would like to thank Dr. Anand Ramanathan, for his expertise in catalyst development and help to me with understanding the relationship between the properties of the catalyst and its performance in reaction.

I would like to thank Dr. Jack Ford and Dr. Haijun Wan for their efforts in building up the main part of the experimental apparatus and guidance of the operation. I would also like to thank Dr. William Kirk Snavely, for his assistance and input in modifying the experimental apparatus and developing the analytical method.

In addition, I appreciate Scott Ramskill for his assistance in the use of Labview program; Ed Atchison and Alan Walker for their kind assistance in the reactor design. I also appreciate Megan Gannon and Claudia Bode, for their assistance in editing the

figures, papers and posters, for this thesis and conference I attended throughout my graduate study.

I would like to thank all my colleagues in CEBC, Dr. Darryl Fahey, Dr. Chris Lyon, Deanna Bieberly, Nancy Crisp, Rhonda Partridge, Dr. Fenghui Niu, Dr. Juan Bravo, Dr. Meng Li, Dr. Zhuanzhuan Xie, Dr. Madhav Ghanta, Wenjuan Yan, Steve Tang, Dupeng Liu, Arely Torres, Xin Jin, Xuchao Li and Xiaohui Hu for the wonderful collaboration experience.

The source of funding for this research was from the U.S Department of Agriculture/National Institute of Food Agriculture (USDA/NIFA).

Finally, I owe so much to my parents, Jianguo Pan and Lingyan Zhang, who were always there standing by me and encouraging me with love, understanding and patience in the good times and bad. I would also like to thank my dearest angel-like sister, Huiru Pan, for being a companion with me throughout the joyful and tough times. Your sense of humor always cheered me up even during the hardest times.

TABLE OF CONTENTS

LIST OF TABLES

LIST OF FIGURES

CHAPTER 1 BACKGROUND AND LITERATURE REVIEW

1.1 Biomass As Renewable Feedstock for Ethylene and Propylene

Ethylene and propylene are considered to be among the most important raw materials in the petrochemical industry. The various uses of ethylene, including as precursor to polymers such as polyethylene, polyvinylchloride and polystyrene, and as raw material for other chemical intermediates such as ethylene oxide, acetic acid and acetaldehyde, make ethylene production capacity one of the indicators to measure the development of the petrochemical industry in countries [Fan 2013 and Zhang 2013]. Propylene, which is considered as the second most important raw material/product in the petrochemical industry after ethylene, serves as the precursor for a wide variety of products such as polypropylene, acrylonitrile, propylene oxide, oxo alcohols and cumene. After experiencing zero growth or declines in 2008 and 2009, global propylene consumption grew at a rate of almost 7.5% in 2010, led by Asia at 11% per year. The world consumption of propylene is forecast to grow with an average rate of 5% per year [IHS Chemical, 2013].

At present, approximately 99% of the global ethylene is produced by steam cracking of hydrocarbons, with petroleum crude or natural gas as raw materials [Zhang, 2013]. Approximately 56% of propylene is produced as a co-product of ethylene manufacture while 33% is produced as a by-product of gasoline production from fluid catalytic cracking (FCC) and 7% of is on-purpose product from the dehydrogenation of propane and metathesis of ethylene and butylene. The remainder (~4%) is from selected gas streams from coal-to-oil processes and from deep catalytic cracking of vacuum gas oil

(VGO). [IHS Chemical-Propylene, 2011]. Clearly, the present global industrial production of ethylene and propylene depends heavily on fossil fuel resources.

Fossil fuel resources are being rapidly depleted to meet the increasing demand for both fuels and chemicals. Alternative raw materials for the production of ethylene and propylene are therefore being actively sought. Non-food biomass is being considered as an important energy source because they not only can reduce net greenhouse gas emissions and dependency on fossil fuels but also represent the only renewable carbon source that can be converted into solid, liquid and gaseous fuels through bio-chemical or thermo-chemical processes [Saxena et al., 2009]. Lignocellulose is a widely used biomass for its abundance and low price. Currently, there are three primary routes to convert lignocellulose to liquid fuels, as shown in Figure 1.1, including gasification to produce syngas, pyrolysis or liquefaction to obtain bio-oil, and hydrolysis to produce sugar monomer units. Presently, an important technology to convert renewable biomass resources into liquid fuels is the production of ethanol (the so-called bioethanol) by fermentation of carbohydrates [Huber, 2006b]. Much work has been done on the production of ethylene by catalytic bioethanol dehydration [Fan, 2013; Vijayalaxmi, 2013; Okajima, 2013; Mazaheri, 2010]. This method has also been applied in industrial production. The Braskem ethanol-to-ethylene plant in Brazil began operation in 2010 and is currently the only plant of its kind at the commercial scale. [Braskem Ethanol-to-Ethylene Plant, 2013].

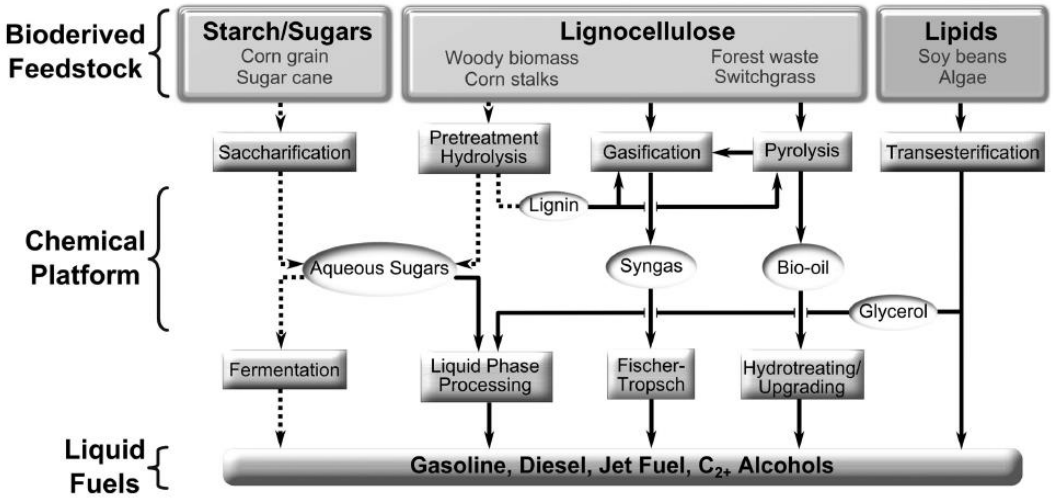

Figure 1.1: Strategies for production of fuels from biomass-derived feedstock [Bravo, 2013]

The high oxygen ratio (40-45 wt%) [Huber, 2006b] in biomass renders the production of hydrocarbons, either fuels or chemicals, rather complex. The controlled removal of oxygen from biomass-based feed stocks is a major challenge. For example, the complexity of compounds in bio-oil (including tars, acids, chars, alcohols, aldehydes, esters, ketones and aromatic) [Huber, 2006b] and in aqueous sugar (including cellulose and hemicellulose, as well as other polysaccharides such as starch and inulin) [Kruger, 2012] make carbon-efficient upgrading to liquid fuels and chemicals particularly challenging.

Two routes can be applied to deoxygenate the biomass: dehydration yielding H_2O; or decarbonylation and decarboxylation, yielding CO and CO_2 respectively [Kruger, 2012]. Dehydration is attractive as an environmental friendly route, because it does not reduce

the number of carbon atoms and does not produce CO_2. Specifically, the olefins produced through dehydration of alcohol can be widely used in the downstream chemical manufacture industry. The challenge for this kind of reaction lies in the fact that high temperature is required for producing olefins from linear bioalcohols via dehydration, side products such as esters and aldehydes also form. Therefore, research in this area has focused on not only the selection of stable mesoporous catalysts that can accommodate large molecules but also catalysts that can selectively produce alcohols in a cost-effective manner. These aspects are further discussed in the following sections.

1.2 Catalysts for Alcohol Dehydration

The dehydration of secondary and tertiary alcohols generally follows the E1 mechanism. As shown in Figure 1.2, the –OH group of alcohol is first protonated by an acid catalyst, followed by loss of water to give carbocation. The conjugate base of the catalyst then removes a hydrogen ion from the methyl group, and the hydrocarbon rearrange into a corresponding olefin. [Fan, 2013]

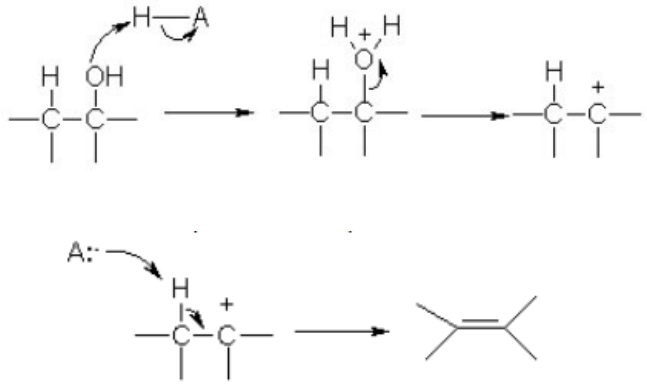

Figure 1.2 Mechanism for the dehydration of alcohol

There are two versions of the mechanism for the dehydration of primary alcohols in literature. One is the E1 mechanism as introduced above [Fan, 2013]. The other is the E2 mechanism according to which the removal of water and hydrogen ion occur simultaneously.

Acid catalysts are generally preferred for E1 mechanism reactions, such as alcohol dehydration to olefins. Both Lewis and Brønsted acid catalysts can be applied for this type of reaction. For example, the conversion of bio-ethanol to ethylene proceeds smoothly over Brønsted acid sites [Bokade, 2011]. However, Brønsted acid sites also catalyze secondary reactions such as cracking and oligomerization leading to the deactivation of such catalysts [West, 2009]. Lewis acid is generally more favorable for high olefin selectivity.

Catalysts for alcohol dehydration can be classified into two major types: (a) microporous catalysts, such as modified alumina [Bakoyannakis, 2001 and Doheim, 2002], supported heteropolyacids [Bokade, 2011], and zeolites [Phillips, 1997; Prestianni, 2013; Takahara, 2005; and Takahara, 2007]; and (b) mesoporous materials such as mesoporous silica. [Jana, 2003; Guan, 2007; Carmona, 2011; Kruger, 2012; and Prabhu, 2013].

1.2.1 Microporous Catalysts

A microporous material is a material containing pores with diameters less than 2 nm [Rouquerol, et al, 1994]. Several studies have been reported for the dehydration of short chain alcohols on microporous catalysts. High conversion and selectivity to olefins was

achieved at relatively mild condition [Chen, Y., et al, 2010; Wu, et al, 2011; and Zhang, 2008]. The Takahara group dehydrated ethanol on a series of zeolites and silica-alumina with SiO_2/Al_2O_3 ratios ranging from 5.6 - 90 in the 180-300 ºC range. The H-mordenites with SiO_2/Al_2O_3 ratio of 90 provided 99.9% ethylene selectivity at 180 ºC [Takahara, 2005]. However, deactivation caused by coke formation hinders commercial application. Further, pore diffusion limitations might also be an obstacle when processing long-chain alcohols.

1.2.2 Mesoporous Catalysts

Mesoporous materials have pore diameter of 2-50 nm [Rouquerol et al, 1994]. Hence, unlike microporous materials, mesoporous materials can accommodate catalytic reactions of larger molecules [Laha et al., 2002]. Ordered mesoporous materials were first introduced with the discovery of the MCM-41 materials by Mobil researchers [Kresge et al., 1992]. Following the discovery of MCM-41, other researchers successfully developed various types of mesoporous materials such as MCM-48 [Vartuli et al., 1994], KIT-1 [Ryoo et al., 1997], SBA-15 [Zhao et al., 1998], TUD-1 [Shan et al., 2000], and KIT-5 [Kleitz et al., 2003]. With the synthesis of these new materials and the supported metallic/molecular species into the mesoporous framework, mesoporous materials have attracted much attention as catalysts for various chemical transformations including oxidation, dehydration and isomerization [Rüfer, 2013].

1.2.2.1 MCM-41 Materials for Dehydration of Alcohols

MCM-41 (Mobile Crystalline Material) is a silicate obtained by a templating mechanism. Arrays of non-intersecting hexagonal channels constitute its basic structure. By changing the length of the template molecule, the width of the channels can be controlled to be within 2 to 8 nm [Kresge, 1992]. Table 1.1 summarizes the use of the MCM-41 materials in alcohol dehydration. The dehydration of both larger alcohols, such as cyclohexanol [Laha *et al.*, 2002] and fructose [Jiang *et al.*, 2011], as well as small alcohols such as methanol [Naik et al., 2010], ethanol, 1-propanol, 2-propanol, 1-butanol [Haishi et al. 2011] and 2-butanol [Kim et al., 2012], have been reported with these catalysts.

The Jana group incorporated aluminum into MCM-41[Jana, 2003]. Most of the acid sites were revealed to be of medium strength by ammonia-temperature-program desorption (NH_3-TPD). Dehydration of 2-propanol was demonstrated producing propylene as the main product. Compared to the microporous catalysts, H-ZSM-5, HY and Al_2O_3, the Al-MCM-41 showed higher activity for 2-propanol dehydration. However, neither the yield of propylene nor information on side products was revealed. The Haishi group reported that the mild acid sites of MCM-41 can control the alcohol dehydration to corresponding olefins. Several alcohols, including ethanol, 1-propanol, 1-butanol, and 2-propanol, were dehydrated on Al-MCM-41. The reported yields of the corresponding olefins are nearly 100% at 430 ºC, 400 ºC, 350 ºC, 280 ºC for ethanol, 1-propanol, 1-butanol and 2-propanol respectively.

Kim et al synthesized WO_3/MCM-41 catalyst with pore sizes ranging from 2.5- 2.65 nm for dehydration of 2-butanol [Kim et al., 2012]. The catalyst contained only weak acid sites. Nearly total conversion of 2-butanol was reported at 300^0C and 1 atm, with 1-butene, trans-2-butene and cis-2-butene as products. In contrast, the alcohol conversion and olefin selectivity values for dehydration over MCM-41 materials with larger molecules including cycolohexanol (1% - 15% in conversion at 200 ºC) [Laha et al., 2002] and fructose (30% - 50% Hydroxymethylfurfural production and no olefin was reported) [Jiang *et al.*, 2011] are relatively low. Further, these reported studies were not aimed at obtaining intrinsic kinetic data, essential to obtain fundamental insights into the reaction mechanism.

The reported drawbacks in using MCM-41 materials as catalyst are as follows: (a) lack of mechanical stability of the amorphous SiO_2 channel walls [Mokaya, 1999]; (b) steric hindrances imposed by typical pore sizes (2-4 nm) to bulky and/or long-chain molecules often encountered when processing biomass-derived substrates.

Table 1.1: Research progress in MCM-41 on dehydration of alcohols

NO.	Catalyst	substrate	Reaction condition			Conversion, %	Yield of product,%	Reaction rate	Reference
			T, ^{0}C	P, atm	t, h				
1	Al-MCM-41-sol gel(Si/Al mole ratio=7)	2-propanol	194	1	Continuous reaction	-	-	0.73 mol/(g h)	Jana *et al.*, 2003
2	Al-MCM-41-hydrothermal (Si/Al mole ratio=7.5)		194	1		-	-	0.46 mol/(g h)	
3	Al-MCM-41-template cation exchange (Si/Al mole ratio = 9)		194	1		-	-	0.93 mol/(g h)	
4	Al-MCM-41-grafting (Si/Al mole ratio=10)		194	1		-	-	0.55 mol/(g h)	
5	MCM-41	MeOH, GHSV=14000 mL/(gcat*h) with He	400	1	Continuous reaction, time on stream 5h	6	6	-	Naik *et al.*, 2010
6	Al-MCM-41		400	1		73	70.8	-	
7	Al-MCM-41 (Si/Al=237)	Ethanol, 0.2g catalyst GHSV=9500h^{-1}, $P_{ethanol}$5.6%	430	1	Continuous reaction, 5 hrs on stream	100	100	-	Haishi *et al.*, 2011
8	Al-MCM-41 (Si/Al=237)	1-propanol, 0.2g catalyst GHSV=16400 /h $P_{1\text{-propanol}}$5%	400	1		100	100	-	

Table 1.1: Research progress in MCM-41 on dehydration of alcohols (Continued)

NO.	Catalyst	substrate	Reaction condition			Conversion, %	Yield of product, %	Reaction rate	Reference
			T, ^{0}C	P, atm	t, h				
9	Al-MCM-41 (Si/Al=237)	1-butanol , 0.2 g catalyst, GHSV=16500/h$P_{1\text{-}butanol}$5.1%	350	1		100	100	-	Haishi *et al.*, 2011
10	Al-MCM-41 (Si/Al=237)	2-propanol, 0.2 g catalyst, GHSV=16400h^{-1}, $P_{2\text{-}propanol}$5%	280	1		100	100	-	
11	27wt% WO_3/MCM-41	2-butanol, 0.01 catalyst 200mL/min N_2	300	1	Continuous reaction	99	trans-2-butene 17%, cis-2-butene 39% and 1-butene 43%	-	Kim *et al.*, 2012
12	2.5% sulfuric acid	10g fructose, 0.5g catalyst, MIBK 50mL, water 50mL	170	1	1.25	87.37	5HMF 35.86%	-	Jiang *et al.*, 2011
13	2% Al-MCM-41		170	1	1.25	60.51	5HMF 32.50%	-	
14	2.5% Al-MCM-41		170	1	1.25	70.56	5HMF 41.70%	-	
15	5% Al-MCM-41		170	1	1.25	72.33	5HMF 42.07%	-	
16	10% Al-MCM-41		170	1	1.25	73.65	5HMF 42.34%	-	
17	5% sulfonated Al-MCM-41		170	1	1.25	83.26	5HMF 51.83%	-	

Table 1.1: Research progress in MCM-41 on dehydration of alcohols (Continued)

NO.	Catalyst	substrate	Reaction condition			Conversion, %	Yield of product, %	Reaction rate	Reference
			T, ^{0}C	P, atm	t, h				
18	Si-MCM-41-R	Cyclohexanol	200	1	1	1	-	-	Laha *et al.*, 2002
19	Ce-MCM-41-R-160		200	1	1	5	-	-	
20	Ce-MCM-41-R-80		200	1	1	11	-	-	
21	Ce-MCM-41-R-40		200	1	1	16	-	-	
22	Ce-MCM-41-R-20		200	1		15	-	-	
23	Ce-MCM-41-P-40		200	1	1	10	-	-	
24	Ce-MCM-41-A-40		200	1	1	8	-	-	
25	Ce-Ex-MCM-41-40		200	1	1	5	-	-	
26	Ce-Im-MCM-41-20		200	1	1	5	-	-	
27	SiO_2-CeO_2-20		200	1	1	3	-	-	

1.2.2.2 SBA-15 Materials for Dehydration of Alcohols

Santa Barbara Amorphous (SBA) type materials are a family of highly ordered mesoporous silicates with pore sizes ranging between 2 and 30 nm. SBA-15 materials possess large BET surface area (>700m^2/g) with tunable pore diameter (up to 12.7 nm) and large pore wall thickness [Kaitiya, 2006]. These features make them suitable for treating bulky biomass substrates. Much fundamental work has been done with SBA materials on dehydrating model compounds of biomass-derivative substrates, including short-chain alcohols (methanol, ethanol, isopropanol, 1-butanol and 2-butanol) over either metal or metal oxide incorporated SBA-15. Table 1.2 summarizes reported SBA-15 materials used in alcohol dehydration.

The Luz group incorporated lanthanum (La) into SBA-15 by a two-stage hydrothermal method and investigated ethanol dehydration over the catalyst. The La incorporation was shown to enhance the acidity compared to Si-SBA-15. The observed ethanol conversion and ethylene selectivity were 65% and 40% respectively at 500 ºC [Luz et al. 2010].

The Carmona and Torres groups investigated SBA-15 supported ZrO_2 and Nb_2O_5 catalysts respectively for isopropanol dehydration [Carmona et al., 2011; Torres et al., 2011]. Both groups reported almost total selectivity towards propylene at 200 ºC and ambient pressure, with the highest conversion (~60%) reported on ZrO_2-SBA-15.

A bifunctional heteropolyacid, 3-((3-(trimethoxysilyl)-propyl)thio)propane-1-sulfonic acid (TESAS) was introduced into SBA-15 and tested it for fructose dehydration to 5-hydroxymethyl furfural (5HMF) [Crisci et al., 2011]. The highest observed fructose

conversion and HMF selectivity were 84% and 71% respectively at 130 ºC and ambient pressure, with a turnover frequency of 0.32 min^{-1}.

The Herrera group synthesized tungsten oxide supported on SBA-15 (WO_x/SBA-15) by atomic layer deposition (ALD) and impregnation methods [Herrera et al., 2006]. Dehydration of methanol and 2-butanol were investigated. For methanol, only dimethyl ether was detected in the product at 300 ºC; in contrast, 1-butene, trans-2-butene and cis-2-butene were detected during 2-butanol dehydration, at 100°C but no ether was detected. Further, the maximum conversion reported was around 50% [Herrera et al., 2006]. More recently, SBA-15 supported rhenium catalysts (ReO_x-SBA-15) were synthesized and tested for 2-butanol dehydration [She et al., 2012]. Almost total conversion is reported at 105 °C with no ether formation. However, catalyst deactivation was fairly rapid as the conversion dropped to ~11% in 230 min.

Table 1.2: Research progress in SBA-15 on dehydration of alcohols

Number	Catalyst	Catalyst to substrate ratio	Reaction condition			Conversion, %	Selectivity of product, %	Reaction rate	Reference
			T, ^{0}C	P, atm	t, h				
1	ALD 1.33 WO_x per nm^2/SBA-15	0.02g catalyst, 0.5kPa 2-butanol, 100.8kPa He, 80 sccm total flow rate	100	1	Continuous reaction, time on stream 3h	-	-	7.2×10^{-4} s^{-1} per W atom	Herrera *et al.*, 2006
2	ALD 0.33 WO_x per nm^2/SBA-15		100	1		-	-	4×10^{-4} s^{-1} per W atom	
3	Imprenated 1.33 WO_x per nm^2/SBA-15		100	1		-	-	7.3×10^{-4} s^{-1} per W atom	
4	ALD 1.33 WO_x per nm^2/SBA-15	0.02g catalyst, 1kPa methanol, 100.3kPa He, 80 sccm total flow rate	300	1	Continuous reaction, time on stream 3h	-	-	3.3×10^{-4} s^{-1} per W atom	Herrera *et al.*, 2006
5	ALD 0.33 WO_x per nm^2/SBA-15		300	1		-	-	3×10^{-4} s^{-1} per W atom	
6	Imprenated 1.33 WO_x per nm^2/SBA-15		300	1		-	-	1.9×10^{-4} s^{-1} per W atom	
7	Zr-SBA-15 (Zr/Si=0.1)	1g catalyst, 8% methanol in volume in a mixture of methanol and N_2 (N_2 flow rate 50mL/min)	350	1	Continuous reaction	20	100	-	Liang *et al.*, 2010
8	Zr-SBA-15 (Zr/Si=0.3)		350	1		59	96	-	
9	Zr-SBA-15 (Zr/Si=0.5)		350	1		70	92	-	

Table 1.2: Research progress in SBA-15 on dehydration of alcohols (Continued)

Number	Catalyst	Catalyst to substrate ratio	Reaction condition			Conversion, %	Selectivity of product, %	Reaction rate	Reference
			T, ^{0}C	P, atm	t, h				
10	Zr-SBA-15 (Zr/Si=0.7)	1g catalyst, 8% methanol in volume in a mixture of methanol and N_2 (N_2 flow rate 50mL/min	350	1	Continuous reaction	65	80	-	Liang *et al.*, 2010
11	Zr-SBA-15 (Zr/Si=0.9)		350	1		60	78	-	
12	Si-SBA-15	60mg catalyst, ethanol as substrate, 37mL/min H_2 as carrier gas	500	1	Continuous reaction, 1.5h	25	40% acetaldehyde, 15% ethylene	-	Luz Jr. *et al.*, 2010
13	La-SBA-15 (Si/La=75)		500	1		55	7% acetaldehyde, 41% ethylene	-	
14	La-SBA-15 (Si/La=50)		500	1		60	10% acetaldehyde, 35% ethylene	-	
15	La-SBA-15 (Si/La=25)		500	1		65	13% acetaldehyde, 30% ethylene	-	
16	$H_3PW_{12}O_{40}$/W-SBA-15	600mg catalyst, glycerol and water mixture 0.056mL/min (10 wt% glycerol), 30mL/min N_2	250	1	Continuous reaction, 24h	100	70% acrolein	-	Kraleva *et al.*, 2011
17	W-SBA-15		250	1		90	70% acrolein	-	

Table 1.2: Research progress in SBA-15 on dehydration of alcohols (Continued)

Number	Catalyst	Catalyst to substrate ratio	Reaction condition			Conversion, %	Selectivity of product, %	Reaction rate	Reference
			T, ^{0}C	P, atm	t, h				
18	3-((3-(trimethoxysilyl)-propyl)thio)propane-1-sulfonic acid (TESAS) into SBA-15	142mg catalyst, 1.5g of 7:3 water/fructose, 3g of 7:3 MIBK:2-butanol	130	1	2.33	84	71% 5HMF	-	Crisci *et al.*, 2011
20	6 weight% CuO/20 weight% CeO_2-SBA-15	25mg catalyst, isopropanol	200	1	Continuous reaction	60	100	-	Reyes-Carmona *et al.*, 2011
21	19 mole% Nb_2O_5/SBA-15 (before water treatment)	100mg catalyst, 2-propanol as substrate, WHSV=15h^{-1} with 20cm^3 (STP) min^{-1} He	180	1	Continuous reaction, 12h	-	-	370	Pagan-Torres *et al.*, 2011
22	HY-340 (before water treatment)		180	1		-	-	114	
23	19 mole% Nb_2O_5/SBA-15 (after water treatment)		180	1		-	-	347	
24	HY-340 (after water treatment)		180	1		-	-	28	
25	ReO_x/AlO_x/SBA-15	20mg catalyst, 0.5% 2-butanol-He, 200mL/min	90	1	Continuous reaction, 3.33h	25	-	-	She *et al.*, 2012
26	ReO_x/AlO_x/SBA-15		105	1		70	-	-	

1.2.2.3 Zr-KIT-6 Materials for Dehydration of Alcohols

KIT-6 materials, first synthesized in 2004, are large pore cubic Ia3d mesoporous silicate, with tunable pore size (4–12 nm) and pore wall thickness (4–6 nm) [Kim, 2004]. The three-dimensional structure of KIT-6 provides more mass transfer channels within the pore structure and also reduces the propensity for pore blockage [Kim et al., 2004; Kleitz et al., 2006; Ramanathan et al., 2013]. These characteristics make KIT-6 materials superior to the one and two-dimensional mesoporous materials such as MCM-41 and SBA-15. Investigations of metal-incorporated KIT-6 are beginning to emerge for applications including epoxidation [Kumaresan , 2010; Vijayalaxmi, 2013],and acylation [Prabhu, 2009]. Recently, the dehydration of cyclohexanol to cyclohexene over cerium incorporated KIT-6 was reported [Prabhu, 2013]. The highest cyclohexanol conversion reported was 54% with 64% cyclohexene selectivity at 300 ºC and 1atm.

Zr has been incorporated into microporous materials such as alumina [Rakshe, 1999] ZSM-5 [Song, 2013] and β-zeolite [Paris, 2013]; and mesoporous materials such as SBA-15 [Chen, 2010] and MCM-41 [El Haskouri, 2002] to enhance catalytic activity as well as stability. Ramanathan et al. synthesized Zr-KIT-6 and report predominantly Lewis acidic sites in the material [Ramanathan, 2013]. This feature makes Zr-KIT-6 a promising catalyst candidate for alcohol dehydration to olefins, given that Lewis acid sites are more favorable for enhancing olefin selectivity as discussed previously in this chapter.

1.3 Scope and Objective

It is clear from the foregoing literature review that numerous efforts are being made to develop advanced mesoporous catalysts for dehydration activity, such as those used to produce olefins from alcohols. In particular, metal-incorporated mesoporous materials show excellent catalytic performance for this kind of reaction. However, the demonstration of a mesoporous catalyst that shows not only high activity and olefin selectivity unhindered by transport limitations but also extended stability to deactivation has remained elusive. Further, systematic kinetic studies are also lacking in the literature. Among the metal-incorporated mesoporous materials, zirconium incorporated KIT-6 material shows promise in meeting the aforementioned challenges. The three-dimensional structure of KIT-6 has the potential to reduce mass transfer limitations and the presence of Lewis acidity that should favor olefin selectivity. Considering these advantages, Zr-KIT-6 was selected as the catalyst for the investigation of alcohol dehydration in this work. The objectives are as follows:

- Investigation of zirconium incorporated KIT-6 (Zr-KIT-6) catalysts with different metal loadings for dehydration of short-chain alcohols, including isopropanol and ethanol in a continuous fixed-bed reactor.
- Study of intrinsic temperature effect on the conversion and the selectivity of the reaction.
- Study of catalyst deactivation during dehydration of each substrate over extended durations.

- Evaluation of intrinsic kinetic parameters based on conversion/selectivity data obtained in the absence of mass transfer limitations.

CHAPTER 2 EXPERIMENTAL REACTOR AND ANALYTICAL EQUIPMENT FOR ISOPROPANOL AND ETHANOL DEHYDRATION STUDIES

2.1 Experimental Apparatus

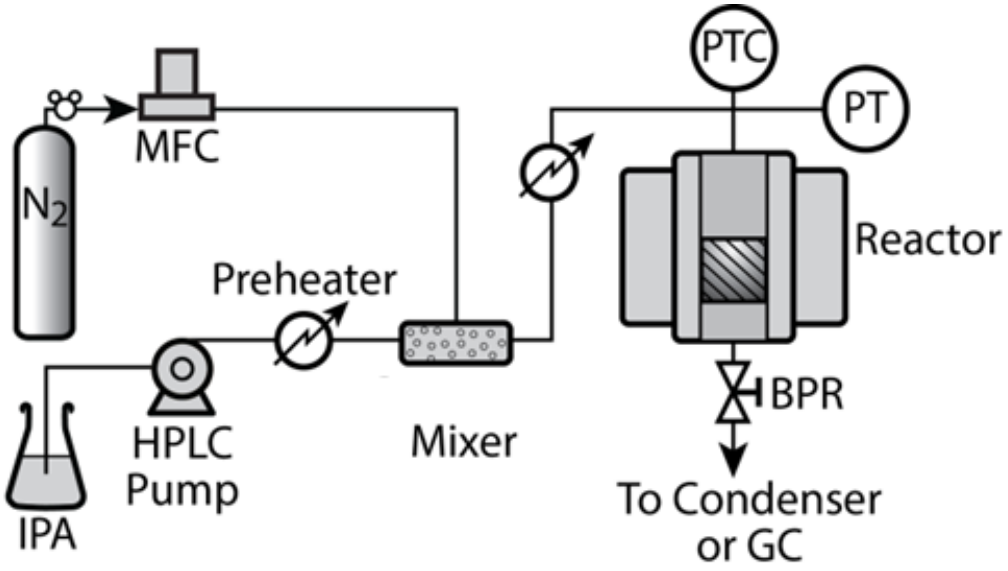

Figure 2.1: Experimental apparatus for dehydration experiments

A schematic of the experimental apparatus is shown in Figure 2.1. The apparatus consists of three main units: the pretreatment unit, the fixed-bed reactor, and the online GC. The pretreatment unit includes a mass flow controller (MFC, Brooks Model 5850E), a HPLC pump (Thermo Separation Products Constametric 3200), a heating cable (Mcmaster-Carr), and an in-line mixer (Thar Designs). The reactor (1 cm ID, 30 cm long), made of Type 304 stainless steel, was heated by Cartridge Heaters (McMaster-Carr. 3618K193), and was covered by cotton insulation (approximately 5 cm thickness) to minimize radial temperature gradients. The reactor temperature was measured with a

profile thermocouple probe (Omega, custom model) placed along the axis of the reactor including six measurement points with a distance of approximately 4 cm between two measuring points. In Figure 2.2, reactor temperature "1" reflects the temperature at the center of the catalyst bed while reactor temperature "2" reflects the temperature at a location that 2 cm away from each end of the catalyst bed. The estimated axial temperature gradient in the 1 cm long catalyst bed is approximately 0.75 ºC. The energy input to the heating cartridge, the reactor temperature, the liquid flow rate through the HPLC pump, and the gas flow rate through the MFC were monitored and controlled by a data acquisition and control module (Measurement Computing, USB-2416-4AO) and LabVIEW version 8.6 software (National Instruments). The automated system allowed for temperature and pressure monitoring at multiple points along the flow path with proportional-integral-derivative control.

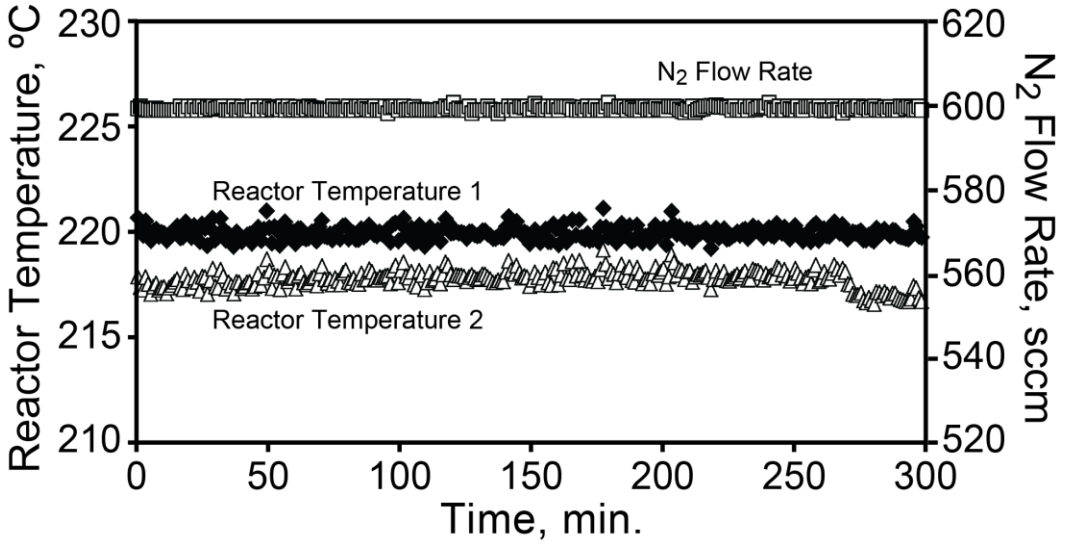

Figure 2.2: Temperature and flow rate control at 220 °C and 300 sccm

Prior to the experiment, the mass flow controller was calibrated with nitrogen using a bubble flow meter. At least three measurements were performed for each set point to ensure accuracy. Table A. 1 and Figure A. 1 (in Appendix A) show the calibration data and curve, respectively.

2.2 Gas Chromatograph

2.2.1 GC Plumbing

An HP 5890 Series II (Agilent Technologies) is used. Figure 2.3 shows the plumbing.

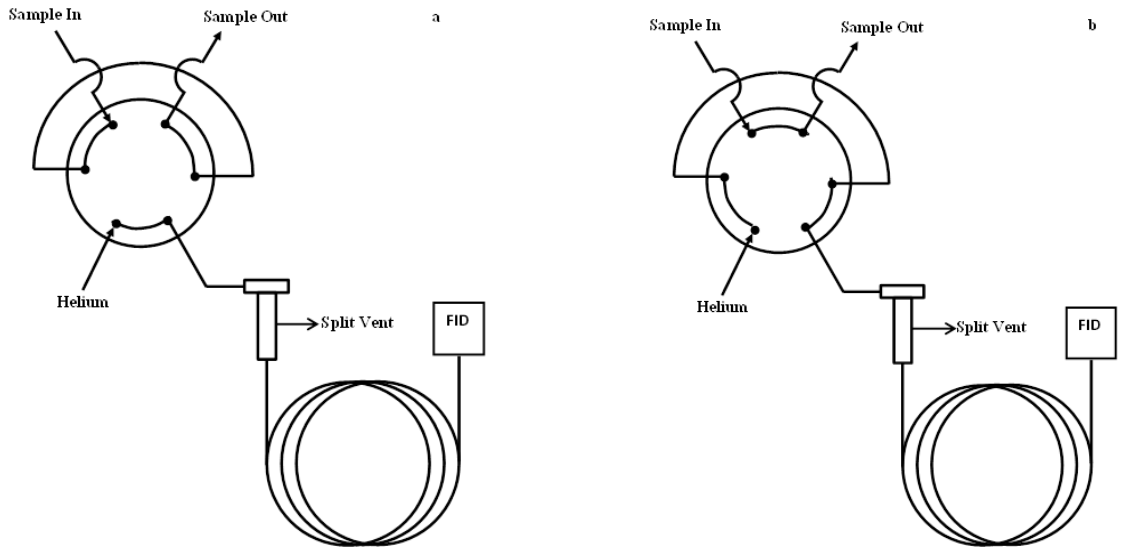

Figure 2.3: Schematic of GC plumbing. (a) normal state; (b) sampling state.

A FID was used to analyze the hydrocarbon products. The injector temperature was set to 250 °C. The GC oven temperature was maintained at 30 °C for the duration of the

analysis (approximately 8 minutes). The FID temperature was set to 300 °C. The H_2 and zero Air flow rates were 25 standard cm^3/min and 500 standard cm^3/min, respectively. A Phenomenex Zebron Phase ZB-WAX capillary column (30 m × 0.25 mm × 0.25 μm) was used to separate the products. The volume of the sample loop is 100 μL and the carrier gas (helium) was flowed at 50 standard cm^3/min.

As the capillary column is easily overloaded, only a small amount of injected analyte is required (McNair, 1998). Therefore, the split/splitless injection ratio was manually set to be 89 with the help of a bubble flow meter to obtain well-resolved peaks of the products.

2.2.2 Qualitative and Quantitative Analysis

Qualitative Analysis

The retention time with standards was used to identify each substance in the outlet stream. A sample chromatogram showing well resolved peaks of propene, IPA, and dipropyl ether is shown in Figure 2.4. A sample chromatogram showing resolved peaks for ethylene, ethanol, diethyl ether, and acetonitrile is shown in Figure 2.5.

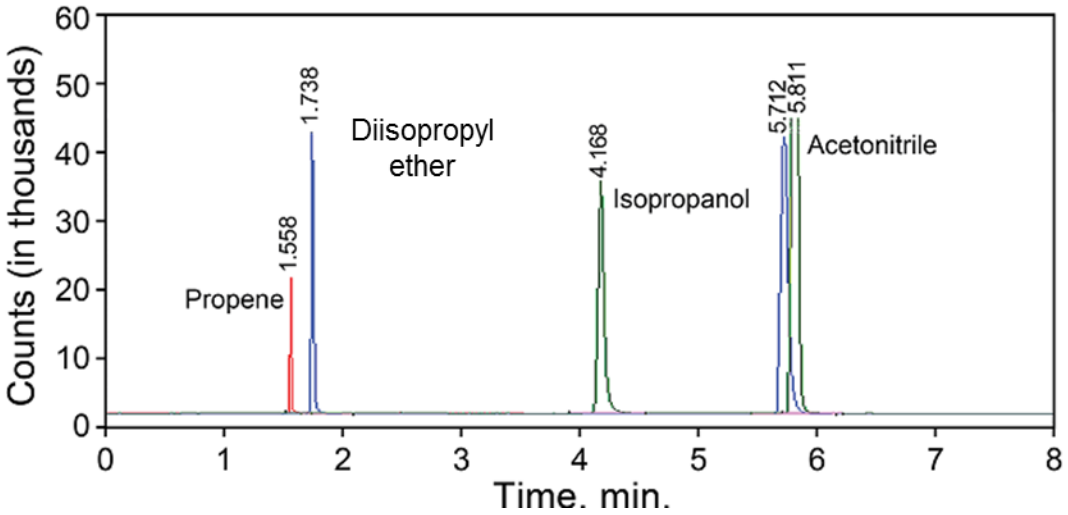

Figure 2.4: GC/FID chromatogram of reactant and products expected during IPA dehydration

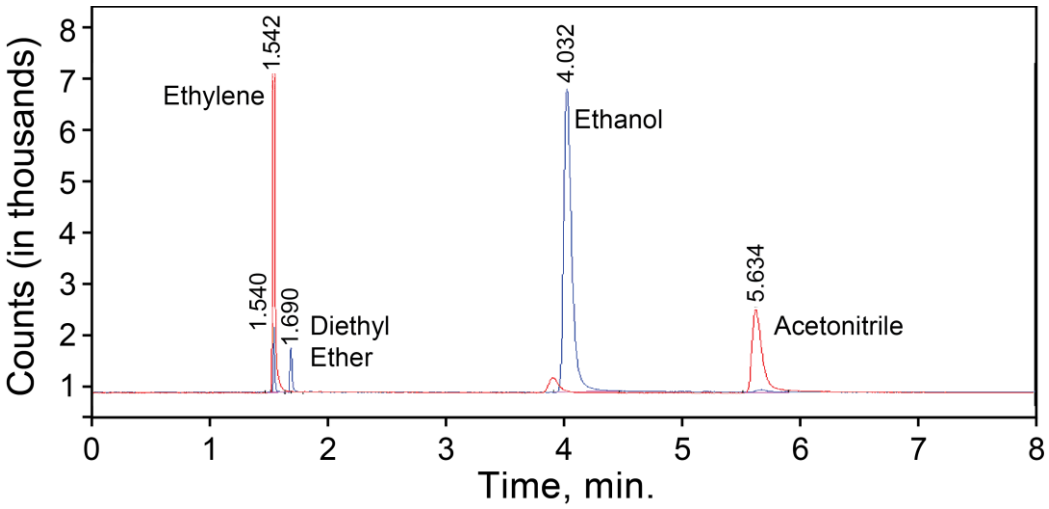

Figure 2.5: GC/FID chromatogram of reactant and products expected during EtOH dehydration

Quantitative Analysis

Internal standardization method was applied for the quantitative analysis. In this method, a known quantity of an inert compound under study is added into the analytes

stream. The ratio of the moles of an analyte present to that of the internal standard is proportional to their area ratio (Eq. 2.1). The proportionality constant is called the response factor. The response factor is obtained by plotting the ratio of the analyte peak area to the internal standard peak area as a function of the ratio of the molar concentrations of the analyte to that of the internal standard (eq. 2.1).

$$\frac{n_i}{n_{st}} = f_i \frac{A_i}{A_{st}} \qquad (2.1)$$

Where, n_i = moles of analyte

n_{st} = moles of internal standard

A_i = peak area of analyte

A_{st} = peak area of internal standard

f_i = response factor.

Acetonitrile (ACN) was considered as the internal standard due to its chemical inertness under reaction conditions. However, it has been reported that strong acid catalysts enhance the hydrolysis of ACN [Barbosa, 2000] with acetic acid as byproduct. Therefore, a test was performed to determine the significance of ACN hydrolysis under typical reaction conditions. The test run duplicates the catalytic runs for either IPA or EtOH dehydration (discussed in Chapter 3) except that the substrate is replaced entirely with water. This is equivalent to the situation when the alcohol is completely dehydrated producing an equivalent molar amount of water as byproduct. Accordingly, a solution of ACN and deionized water with a molar ratio of approximately10:1 (identical to the molar IPA/ACN ratio used in the experiments) was fed to the reactor by a Thermo Separation Products Constametric 3200 Pump at a typical flow rate of 0.1 cm^3/min. Prior to entering

an in-line mixer and mixing with N_2, the pumped liquid mixture was vaporized by preheating to 150 °C. Nitrogen was fed through a solenoid valve and metered into the in-line mixer with the mass flow controller at predetermined flow rates of 600 standard cm^3/min (sccm). The combined ACN solution/N_2 feed mixture was then introduced as vapor into the reactor and passed over 1.5 g of the most acidic catalyst sample [Zr-KIT-6 (20)]. The test run was performed in the 100- 400 ºC range at 1 atm reactor pressure.

Figure 2.6 shows the variation of the ACN peak area with temperature. No other peaks besides the ACN peak were found on the chromatograph. Each run was conducted for 2.5 h. The peak area was the mean of 4 measurements. Although the peak area fluctuated (± 15 %) because of variations in the injection amounts, there is no discernible decreasing trend as the temperature increased confirming that ACN may be considered inert over the Zr-KIT-6 catalysts.

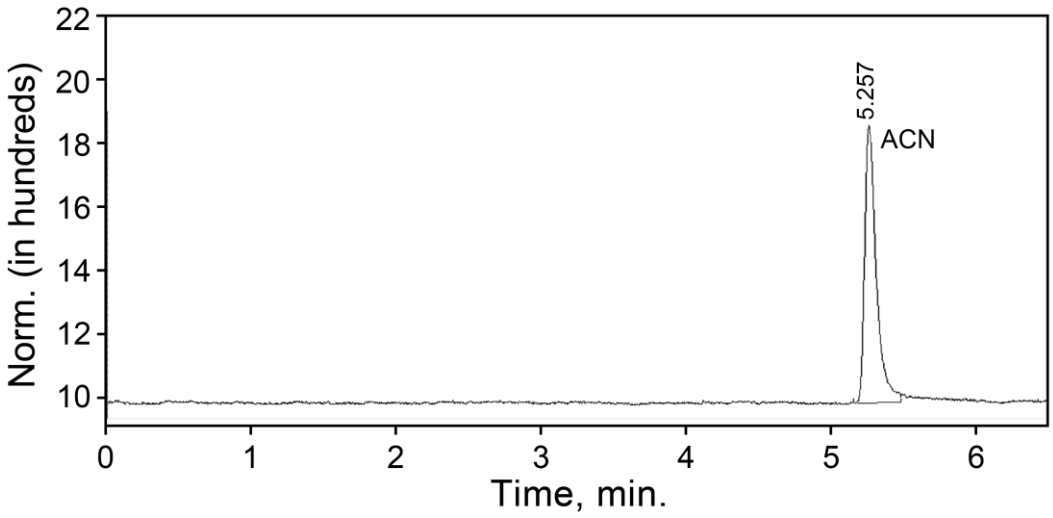

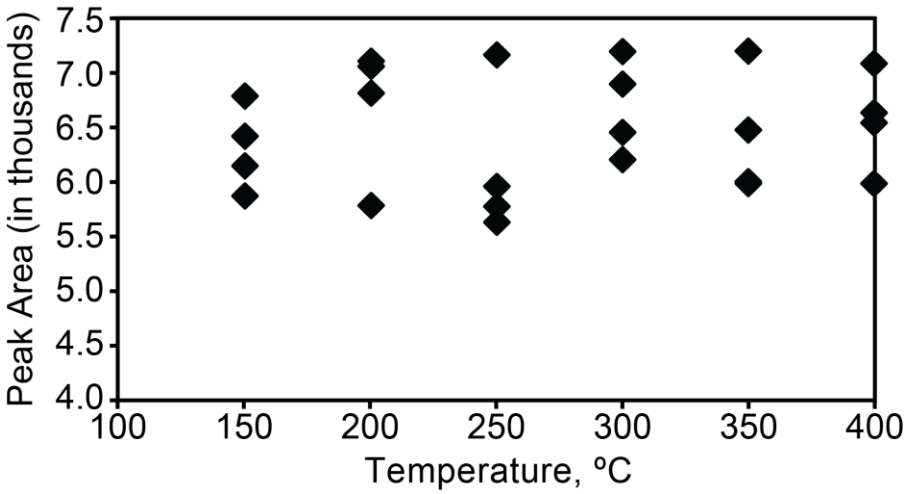

Figure 2.6: (a) GC chromatogram of ACN hydrolysis test; (b) ACN peak area with temperature. The test was conducted at 1 atm for 2.5 h at each temperature, GHSV = 7,200h^{-1}.

Calibrations of propene and ethylene were performed by online injection using the same apparatus as shown in Figure 2.1. The nitrogen cylinder was replaced by the standard gas cylinder (5 mole% propene in N_2). The flow rate of the standard gas was accurately controlled by the MFC and monitored using Labview®. Pure acetonitrile was pumped at a certain flow rate (set and monitored by Labview® as well) by the HPLC pump, preheated before mixing with the standard gas stream. The mixed stream then passed through the empty reactor and was analyzed in the GC.

Calibrations of liquid compounds (IPA, ethanol, dipropyl ether, and diethyl ether) were conducted by manual injection of the standard samples. A series of liquid standard samples with known molar ratios of target compounds and acetonitrile was prepared. At least five injections of standards in series were made for each compound to ensure

accuracy. For manual injection, the sample was injected directly into the capillary column from the manual injection port without split. Therefore, the samples were further diluted in acetone to avoid overloading. Each sample (1 µL) was injected using a Hamilton microliter syringe (10 µL, 701N, 80300). At least three repeat injections were made for each sample to check for reproducibility. Molar ratio versus peak area curves were generated for calibration purposes. The calibration curves and the associated data sheet are shown in Appendix A.

CHAPTER 3 DEHYDRATION OF ISOPROPANOL AND ETHANOL OVER Zr-KIT-6 MATERIALS

3.1 Experimental

3.1.1 Chemicals

Solvents including isopropanol (99.9%), dehydrated ethanol (99.5%), acetonitrile (99.9%), diethyl ether (99.9%), dipropyl ether (99.9%), and acetone (99.5%) were purchased from Fisher Scientific and used as received. Zirconia nanopowder was purchased from Sigma-Aldrich. Helium (ultra-pure grade), nitrogen (industry grade) and air (industry grade) were purchased from Matheson Linweld.

The Zr-KIT-6 material used in this study was synthesized and characterized as reported elsewhere [Ramanathan, 2013]. Three samples with different Zr loading were investigated for dehydration activities. Table 3.1 shows the properties of the samples.

Table 3.1 Properties of the Zr-KIT-6 catalyst samples

Zr-KIT-6(Si/Zr)[a]	Si/Zr [b]	Zr [b]	a_0 [c]	S_{BET} [d]	$V_{p,BJH}$ [e]	$d_{P,BJH}$ [f]	W[g]	Total Acidity
		wt%	nm	m^2/g	cc/g	nm	nm	(NH_3 mmol/g)
100	92	1.6	24.3	980	1.65	9.3	3.7	0.19
40	39	3.8	24.6	881	1.42	9.3	4.4	0.40
20	23	6.2	25.7	810	1.07	9.3	4.4	0.49

[a] numbers in parenthesis represent Si/Zr ratio in synthesis gel, [b] ICP-OES analysis

[c] $a_0 = d_{211} / \sqrt{(h^2+k^2+l^2)}$, [d] S_{BET} = Specific surface area.

[e] $V_{P,BJH}$ = Total Pore Volume measured at 0.995 $P/P_{o,}$

[f] $d_{P,BJH}$ = BJH adsorption Pore Diameter, [g] W = wall thickness evaluated by $a_0/2 - D_{P,DFT}$

3.1.2 Experimental Procedure for Isopropanol (IPA) and Ethanol (EtOH) Dehydration Studies

The catalytic dehydration reactions were carried out in a continuous fixed-bed reactor over Zr-KIT-6 catalysts which were pelletized to 250-700 nm. The performance of three Zr-KIT-6 materials with different zirconium contents (Si/Zr ratio of 20, 40, and 100) for IPA and EtOH dehydration was investigated. Specifically, conversion and selectivity data on these catalysts were compared in the 190-300 °C range for IPA and 300-380 °C range for EtOH at atmospheric pressure. Approximately 1.5 g of the catalysts was packed with two screens at each end as holders to ensure reproducible packing position. A solution of IPA (or EtOH) and acetonitrile (ACN) with a molar ratio of approximately 10:1 was fed to the reactor by means of the HPLC pump at a typical flow rates of 0.1 cm^3/min. Prior to entering an in-line mixer and mixing with N_2, the pumped liquid mixture was vaporized by preheating to 150 °C. Nitrogen was fed through a solenoid valve and metered into the in-line mixer with the mass flow controller at predetermined flow rates ranging from 200-800 standard cm^3/min (sccm). The combined IPA (or EtOH)/N_2 feed mixture was then introduced as vapor into the reactor. Downstream from the reactor, the effluent stream containing the unreacted reactants and products was kept vapor phase of 160 °C by the heating cord and was sampled online to a 5890 Series II gas chromatograph. And the products were analyzed with a Phenomenex Zebron Phase ZB-WAX capillary column (30 m x 0.25 mm x 0.25 μm) and a flame ionization detector. Two replicate runs were conducted on each catalyst. The measurement range and precision of various measuring instruments are listed in Table 3.2.

Table 3.2: Instrument measurement ranges and precision

Instrument	Measurement Range	Precision
Electronic Scale	0 ~ 210 g	± 0.1 mg
Micrometer syringe	0 ~ 10 µL	± 0.01 µL
Thermocouple	0 ~ 400 ºC	± 0.5 ºC
Mass flow controller	0 ~ 1500 sccm	± 1 sccm
HPLC Pump	0 ~ 10 mL/min	± 0.001 mL/min

3.2 Catalytic Dehydration of Isopropanol (IPA) over Zr-KIT-6 Catalysts

3.2.1 Conversion/Selectivity Results

Figure 3.1 shows a typical chromatograph of the IPA dehydration with GC analysis.

The following definitions were used in presenting the results. Conversion (X) is defined as the ratio of the moles of IPA converted to the moles of IPA in the feed stream. Selectivity (S) is defined as the ratio of the moles of propene formed to the moles of IPA converted. The gas hourly space velocity (GHSV) is defined as the total gas feed rate at ambient conditions per catalyst volume (h^{-1}).

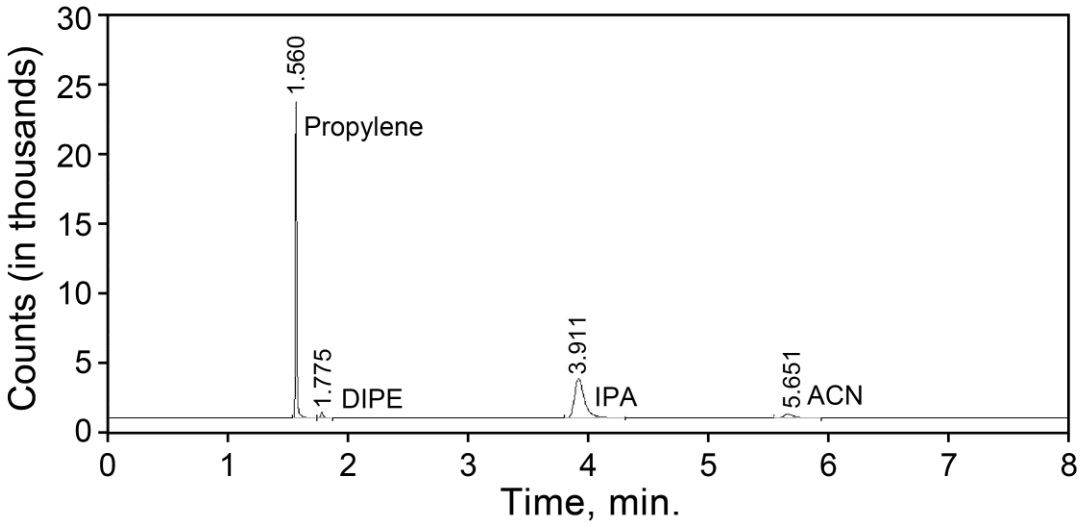

Figure 3.1 Sample chromatogram of the effluent stream during IPA dehydration over Zr-KIT-6 (20), T = 260 °C, GHSV = 7,200 h^{-1}, p = 1 atm.

Figure 3.2 shows the variation of steady state IPA conversion and propene selectivity with temperature at a fixed space velocity for the various Zr-KIT-6 materials tested. The plotted values represent average conversion and selectivity data collected at steady state between three and five hours. For all the three Zr-KIT-6 materials tested, the conversion increased with temperature as expected, reaching nearly total conversion at 300 °C. Furthermore, at a given temperature, the conversion increased with Zr content (i.e., acidity) of the catalyst sample. In contrast, the IPA conversion on ZrO_2 was relatively low, reaching only around 10% even at 300°C. The selectivity to propene was greater than 98.5% for all Zr-KIT-6 samples and independent of conversion. The propene selectivity is higher than the 39-78% range reported on predominantly Lewis acidic catalysts such as Al_2O_3 and ZrO_2 [Turek, 2005].

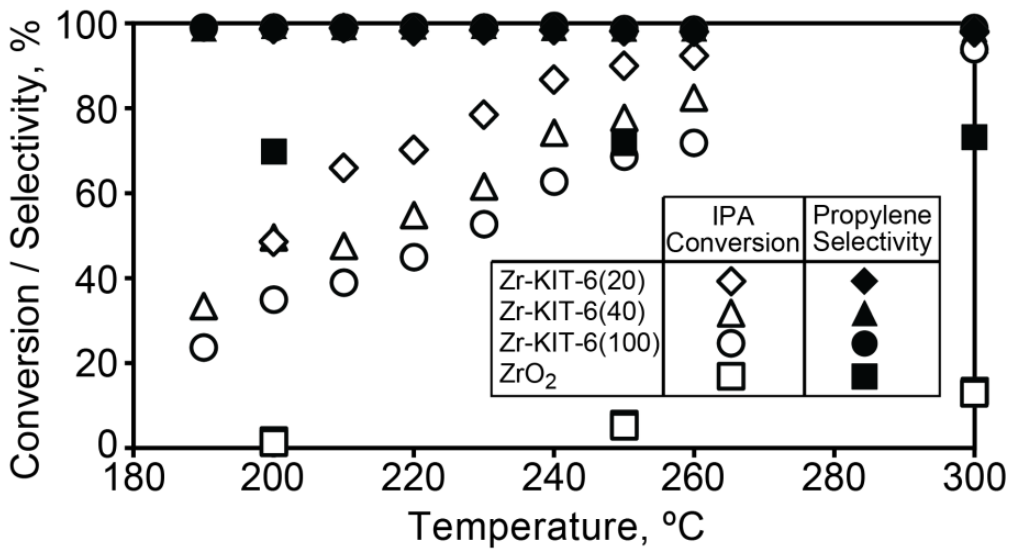

Figure 3.2: Effect of temperature on IPA conversion and propene selectivity. IPA in feed = 5 mole% in N_2; Catalyst loading = 1.5 g; GHSV = 7,200 h^{-1}, p = 1 atm.

3.2.2 Determination of Intrinsic Kinetic Parameters

Effective rate constants were estimated from the measured steady state conversions. Given the high propene selectivity (>98.5%), only the dehydration reaction was considered. Further, since N_2 was the dominant component (>95 mole%), the volume change upon reaction is ignored as being insignificant. Based on these assumptions, an effective first-order rate constant (k_e) based on a plug flow reactor model is given by Eq.3.1.

$$k_e = -\frac{v_g}{V_c}\ln(1 - X_A) \qquad \text{(Eq. 3.1)}$$

Where, k_e = effective rate constant (min^{-1})

v_g = volumetric flow rate at reactor P and T (cm^3/min)

V_c = packed volume of catalyst (cm^3)

X = observed IPA conversion at steady state.

As shown in Figure 3.3, the effective rate constants increased at relatively low GHSV values and became invariant above approximately 6,000 h^{-1} at 260 °C. This indicates that external mass transfer limitations were eliminated.

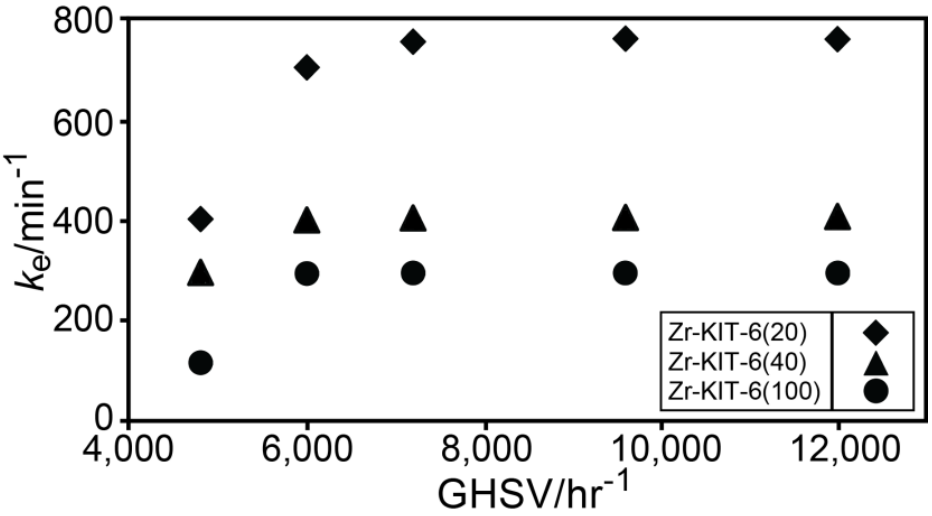

Figure 3.3: The dependence of effective rate constant (k_e) on GHSV at 260 °C, 1 atm.

In addition, catalyst effectiveness factors (η) were estimated using well-known correlations (Eq. 3.1) [Cussler 2nd Ed. 1997] for spherical pellets under conditions where external mass transfer limitations are eliminated. The calculated effectiveness factors (Table 3.3) were above 0.998 for all the catalyst samples and runs (Detailed calculation is in Appendix B). The absence implies that, above 6,000 h^{-1}, both external and internal mass transfer limitations are eliminated and that the IPA reaction is controlled by intrinsic kinetics.

Table 3.3: Dependence of effectiveness factor on GHSV for IPA dehydration at 260 °C, 1 atm

GHSV h^{-1}	η Zr-KIT-6 (20)	Zr-KIT-6 (40)	Zr-KIT-6 (100)
2400	0.9996	0.9997	0.9999
4800	0.9993	0.9995	0.9998
6000	0.9987	0.9993	0.9995
7200	0.9987	0.9993	0.9995
9600	0.9986	0.9993	0.9995
12000	0.9986	0.9993	0.9995

Estimation of Intrinsic Activation Energy

In order to estimate the intrinsic activation energy, the reactions were conducted at temperatures ranging from 200 – 260 °C employing a GHSV of 7,200 h^{-1} wherein both external and internal mass transfer limitations are eliminated. As shown in Figure 3.4a, the Zr-KIT-6 samples with higher Zr content yielded higher rate constants when such rate constants were normalized with respect to the volume of the catalyst packing (Eq. 3.1). However, when the rate constants were normalized with respect to the total acidity of the respective Zr-KIT-6 materials (Eq. 3.7), the rate constants at the various temperatures virtually overlapped for all the catalysts, suggesting that the dehydration reaction occurs on the Lewis acid sites (Figure 3.4b).

$$k'_e = -\frac{\nu_g}{A_c w_c} \ln(1 - X) \qquad \text{(Eq. 3.7)}$$

Where, k'_e = *intrinsic kinetic rate constant* (min^{-1})

ν_g = volumetric flow rate at reactor P and T (cm^3/min)

w_c = weight of catalyst used (g)

A_c = total acidity of catalyst [(cm^3 NH_3 at standard conditions)/g catalyst]

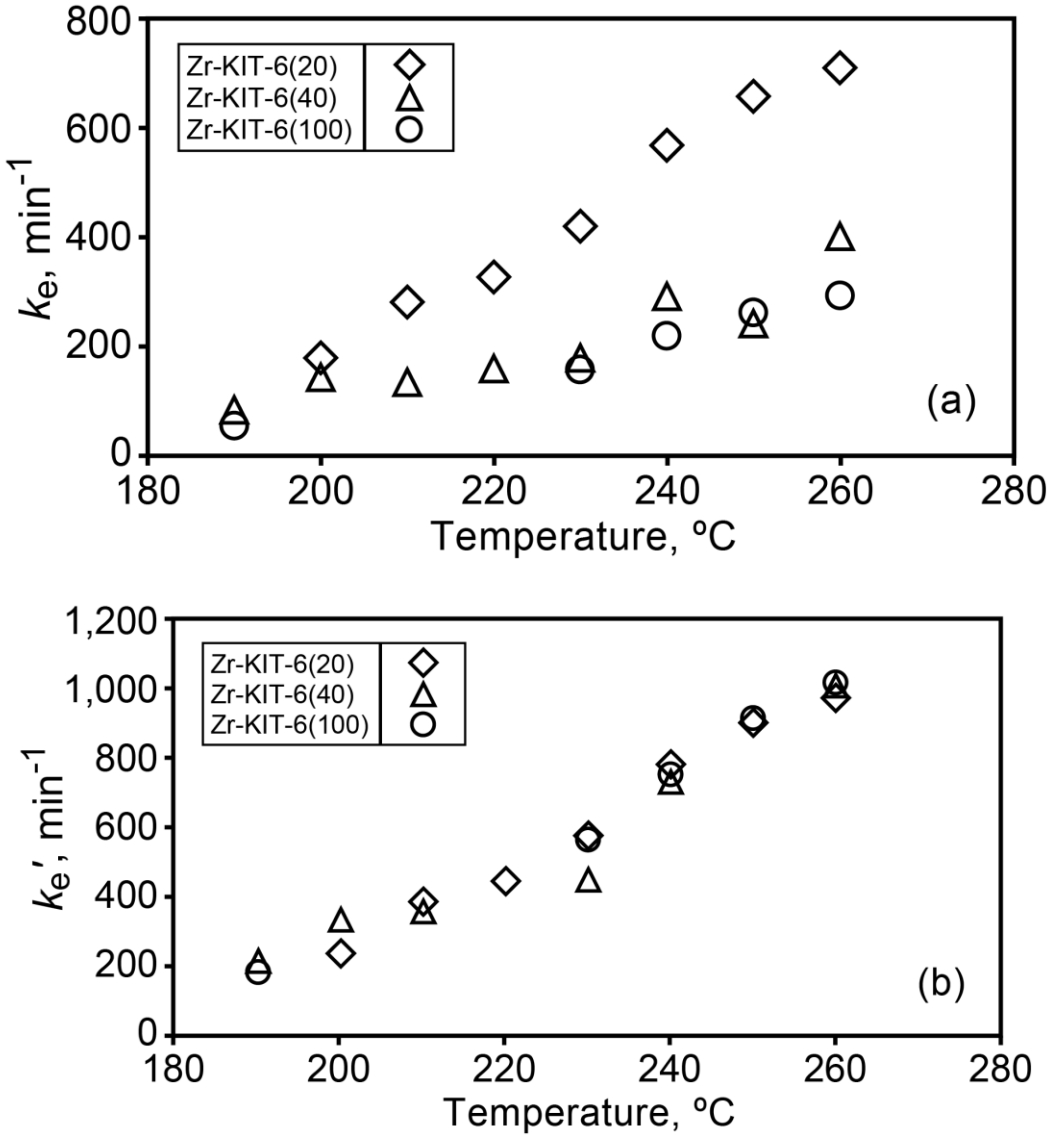

Figure 3.4 Dependence of rate constant with temperature. (a) intrinsic rate constants (k_e) based on catalyst packing volume, and (b) intrinsic rate constants (k_e') based on catalyst acidity.

The activation energy was estimated from the Arrhenius equation (Eqs. 3.8 and 3.9)

$$k = Ae^{-\frac{E_a}{RT}} \quad \text{(Eq. 3.8)}$$

$$lnk = \ln A - \frac{E_a}{R}\frac{1}{T} \quad \text{(Eq. 3.9)}$$

Where, k = rate constant (s^{-1})

E_a = activation energy (J/mol)

A = pre-exponential factor (s^{-1})

T = Catalyst temperature (K)

R = universal gas constant [8.314 J/(mol·K)]

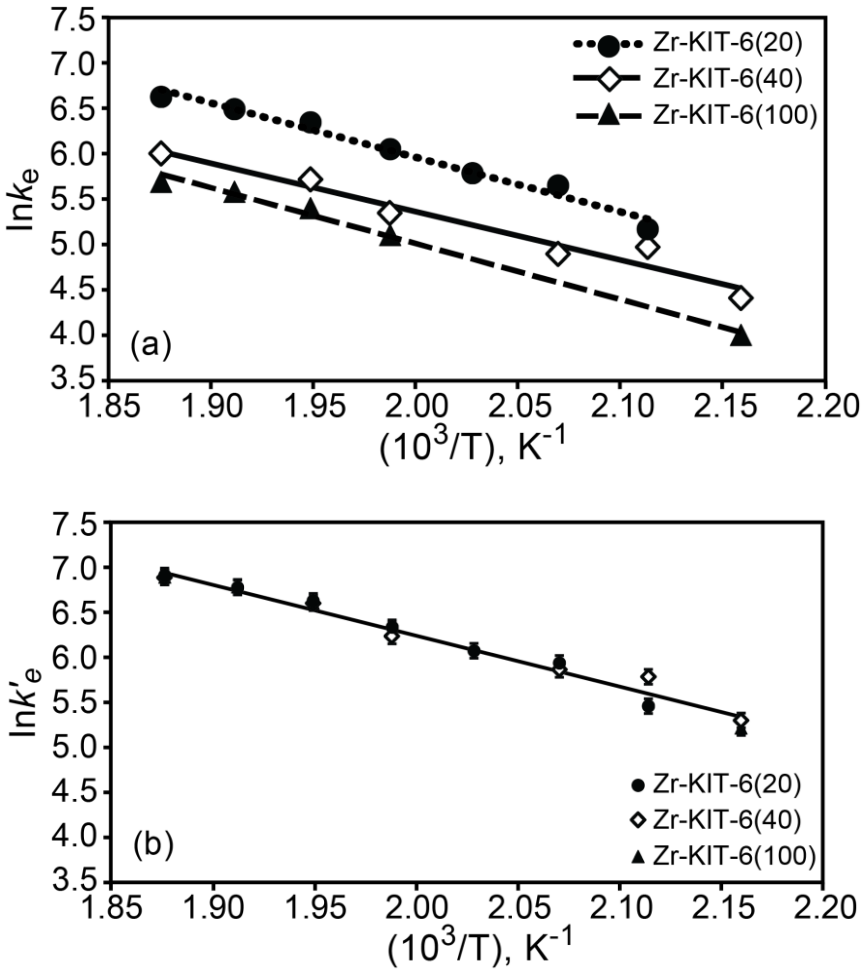

Figure 3.5: Estimation of activation energy for dehydration of IPA from (a) intrinsic rate constants (k_e) based on catalyst packing volume, and (b) intrinsic rate constants (k_e') based on catalyst acidity.

Considering the effective rate constants, the activation energy in each case was approximately 45-50 kJ/mol (Figure 3.5a). The intrinsic activation energy based on acidity-normalized rate constants was estimated to be approximately 48.9 ± 0.5 kJ/mol (Figure 3.5b). As compared in Table 3.4, this value is generally lower than those reported for IPA dehydration on solid acid catalysts that contain predominantly either Brønsted acid sites (40-120 kJ/mol on bulk and supported heteropolyacids) [Bond, 2012] or Lewis acid sites (133 kJ/mol on γ-Al_2O_3 and 173 kJ/mol on ZrO_2) [Turek, 2005].

Table 3.4: Comparison of activation energies for isopropanol dehydration over Zr-KIT-6 catalyst with those reported in the literature

Catalyst	E (kJ/mol)	Reference
Bulk $H_3PW_{12}O_{40}$(HPW) Acid	104	[Bond, 2012]
Bulk $Cs_nH_{3-n}PW$ Acid	68	[Bond, 2012]
15% HPW-ZrO_2	59	[Bond, 2012]
15% HPW-TiO_2	90	[Bond, 2012]
15% HPW-SiO_2	86	[Bond, 2012]
15% HPW-Nb_2O_3	43	[Bond, 2012]
Bulk $H_3PMo1_2O_{40}$	117	[Turek, 2005]
γ-Al_2O_3	173	[Turek, 2005]
ZrO_2	133	[Turek, 2005]
Zr-KIT-6 (This work)	49	-

3.2.3 Catalyst deactivation test

A 30 h extended run with Zr-KIT-6(20) at 260°C (Figure 3.6a) showed slight deactivation with the IPA conversion dropping from 93.2% to 91.5%. Similarly, Zr-KIT-

6(40) and Zr-KIT-6(100) samples were tested at 300°C for 12 h and little deactivation was observed: the IPA conversion decreased from 97.3 to 96.1% for Zr-KIT-6 (40), but remained constant at approximately 94% for Zr-KIT-6 (100) (Figure 3.6b). The decrease in the rate constant with time for the various catalysts is less than 1%/h summarized in Table 3.5. These values range between 0.27%/h to 0.83%/h demonstrating that the tunable Lewis acidity of the Zr-KIT-6 materials favors high conversion and propene selectivity with relatively low formation of the major byproduct (dipropyl ether) and enhanced stability compared to other reported catalysts.

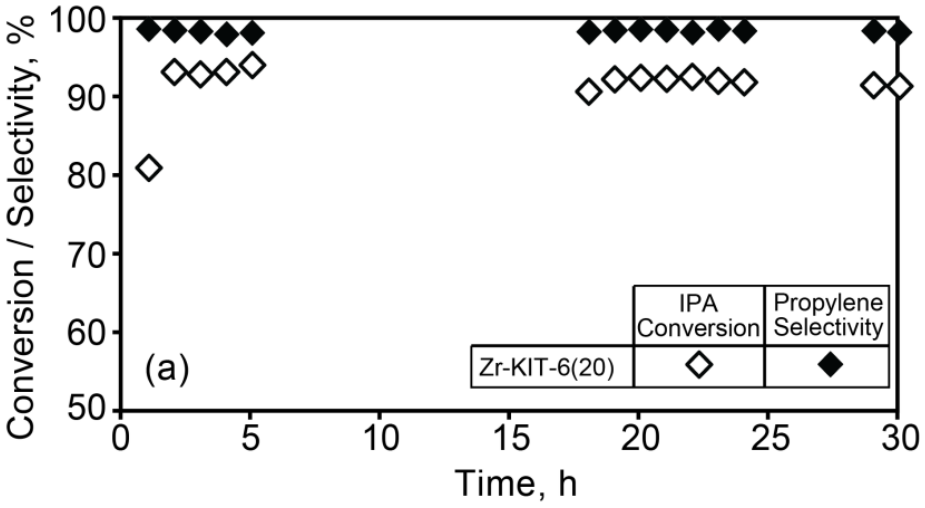

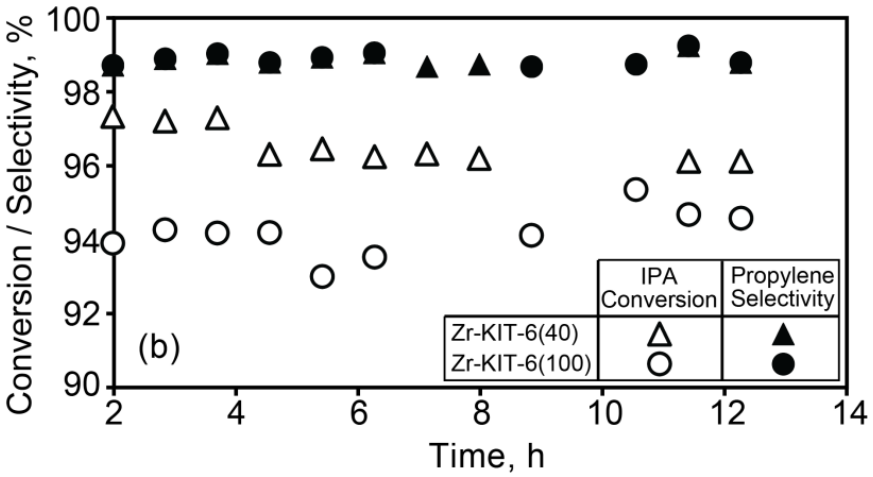

Figure 3.6: Stability test over Zr-KIT-6 samples with IPA dehydration. (a) 30 h run on Zr-KIT-6(20) at 260°C; (b) 12 h run on Zr-KIT-6(40) and Zr- KIT-6(100) at 300°C. IPA in feed = 5 mole% in N_2; Catalyst loading = 1.5 g; GHSV = 7,200 h^{-1}; p = 1 atm.

Table 3.5: Deactivation rate in terms of effective rate constant decreasing percentage

Catalyst Sample	T	Initial k_e	Final k_e (after *t* hours)	Deactivation rate (Initial k_e – Final k_e)/t
	ºC	min^{-1}	min^{-1}	%/h
Zr-KIT-6 (20)	260	583.2 ± 8.6	538.3 ± 5.0	0.27
Zr-KIT-6 (40)	300	891.6 ± 6.1	802.9 ± 0.1	0.83
Zr-KIT-6 (100)	300	703.6 ± 3.2	722.2 ± 2.3	-

3.3 Catalytic Dehydration of Ethanol (EtOH) over Zr-KIT-6

3.3.1 Conversion/Selectivity Results

Figure 3.7 shows a typical GC chromatograph of the EtOH dehydration products.

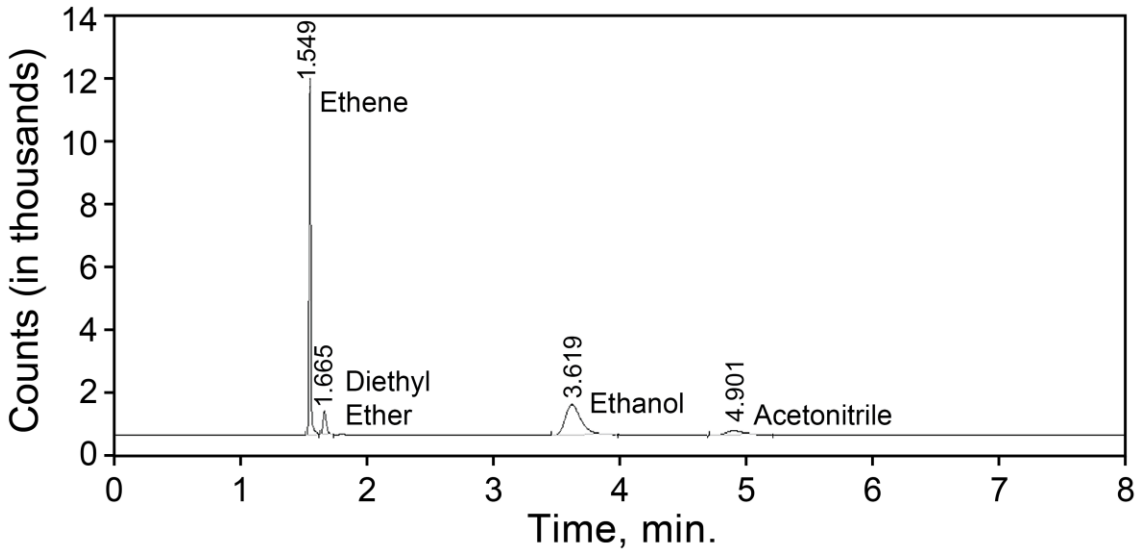

Figure 3.7 Sample chromatogram of the effluent stream during EtOH dehydration over Zr-KIT-6 (20), T=260 °C, GHSV=7,200 h^{-1}, p=1 atm

The effects of temperature on EtOH conversion and ethylene selectivity on Zr-KIT-6 materials and commercial ZrO_2 were investigated. Average conversion and selectivity data were taken after the reaction reached steady state at each temperature (in approximately 2 - 4 hours). As shown in Figure 3.8, the steady-state conversion slightly increased with temperature. There was no significant superiority of the Zr-KIT-6 materials over commercial ZrO_2 with respect to ethanol conversion, which ranged from 15% -30%. However, the selectivity to ethylene was in the range of 60% - 80% for Zr-KIT-6 materials, which was greater than the ethylene selectivity obtained with commercial ZrO_2 (around 40%).

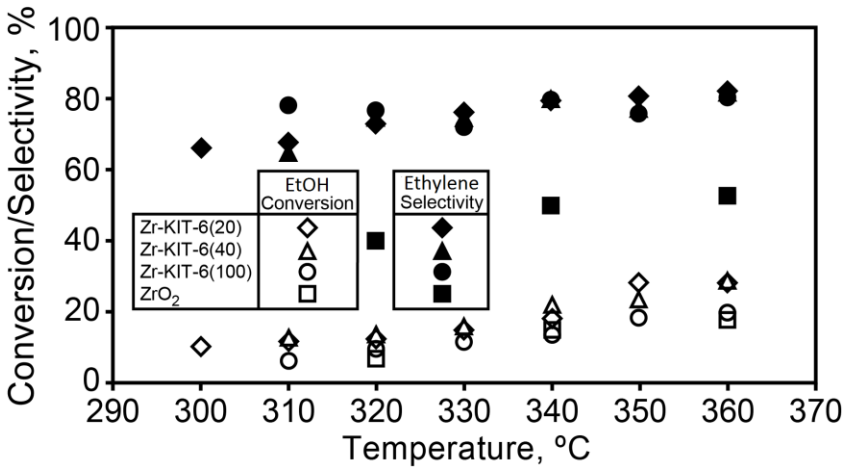

Figure 3.8: Effect of temperature on EtOH conversion and ethylene selectivity. EtOH in feed = 5 mole% in N_2; Catalyst loading = 1.5 g; GHSV = 7,200 h^{-1}, p = 1 atm

Figure 3.9 shows a 70 h extended run with Zr-KIT-6(100) at 380°C. The conversion and selectivity were steady within the first 30 hours. Between 40 to 60 hours, the conversion slightly increased, while the selectivity decreased. After 60 hours, the conversion and selectivity dropped by approximately 67% and 77%, respectively.

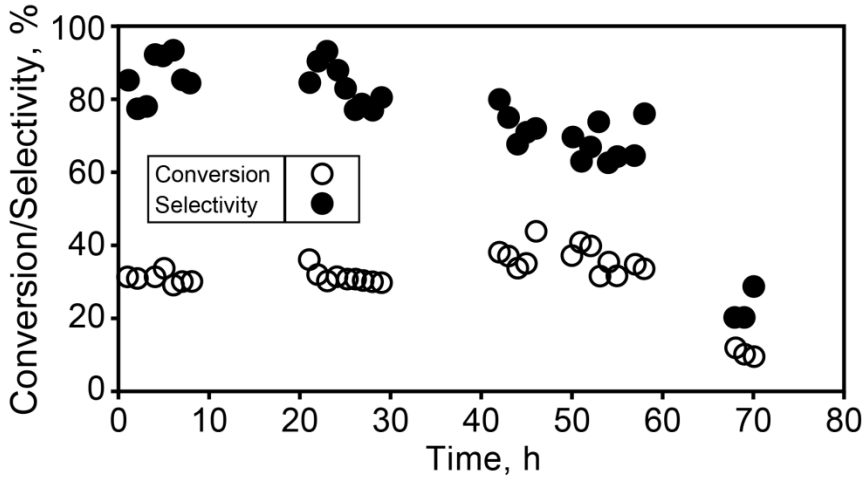

Figure 3.9: 70 h stability test on Zr-KIT-6(100) at 380°C EtOH in feed = 5 mole% in N_2; Catalyst loading = 1.5 g; GHSV = 7,200 h^{-1}, p = 1 atm.

3.3.2 Kinetic analysis of EtOH dehydration on Zr-KIT-6

As the ethylene selectivity for the EtOH dehydration was only around 80%, the side reaction involving diethyl ether formation must be taken into account. The stoichiometries for the dehydration (Reaction 1) and dehydrogenation (Reaction 2) reactions are as follows.

C_2H_5OH (A) $\longrightarrow$ C_2H_4 (B) + H_2O (C) (Reaction 1)

2 C_2H_5OH (A) $\longrightarrow$ C_2H_5-O-C_2H5 (D) + H_2O (C) (Reaction 2)

For developing the kinetic model, the two parallel reactions are assumed to be first-order in substrate concentration. The steady state material balance equations are derived as follows.

$$-\frac{dF_A}{dV_c} + r_A = 0 \quad \text{(Eq. 3.10)}$$

Where, $-\frac{dF_A}{dV_c} = C_{A_0} v_g \frac{dX_A}{dV_c}$

$r_A = -(k_{e1}C_A + k_{e2}C_A)$

$C_A = C_{A_0}(1 - X_A)$

Therefore, Eq. 3.10 can be further rewritten as Eq. 3.11

$$v_g \frac{dX_A}{dV_c} = k_{e1}(1 - X_A) + k_{e2}(1 - X_A) \quad \text{(Eq. 3.11)}$$

For Reaction 1, $v_g \frac{dX_{1A}}{dV_c} = k_{e1}(1 - X_{1A} - X_{2A})$, where, $X_{1A} = S_1 X_A$

For Reaction 2, $v_g \frac{dX_{2A}}{dV_c} = k_{e1}(1 - X_{1A} - X_{2A})$, where, $X_{2A} = S_2 X_A$

Combining equations 3.10 and 3.11 and integrating, the rate constants for Reaction 1 and 2 are given by

$$k_{e1} = -\frac{v_g S_1}{V_c} \ln(1 - X_A) \quad \text{(Eq. 3.12)}$$

$$k_{e2} = -\frac{v_g S_2}{V_c} \ln(1 - X_A) \quad \text{(Eq. 3.13)}$$

Where, k_{e1} = effective rate constant for Reaction 1 (min^{-1})

k_{e2} = effective rate constant for Reaction 2 (min^{-1})

v_g = volumetric flow rate at reactor P and T (standard cm^3/min)

V_c = packed volume of catalyst (cm^3)

X_A = observed EtOH conversion at steady state

S_1 = selectivity toward ethylene at steady state

S_2 = selectivity toward diethyl ether at steady state

Equation 3.12 was applied to calculate the rate constant for EtOH dehydration. In order to assess the effect of external mass transfer limitations, a series of experiments was conducted over the most acidic catalyst sample, Zr-KIT-6 (20) at 360 and 380 °C and at different GHSV values at each temperature. As shown in Figure 3.10, over Zr-KIT-6 (20), the effective rate constants kept increasing with GHSV at 380 °C, while they reached a plateau above GHSV values of 7,000 h^{-1} at 360 °C. Furthermore, the calculated effectiveness factors were above 0.99 within the tested GHSV range and temperatures (Figure 3.11). Therefore, it is concluded that on all the Zr-KIT-6 materials tested, both the external mass transfer limitations as well as intraparticle diffusion limitations are eliminated above GHSV values of 7,000 h^{-1} at temperatures below 360 °C.

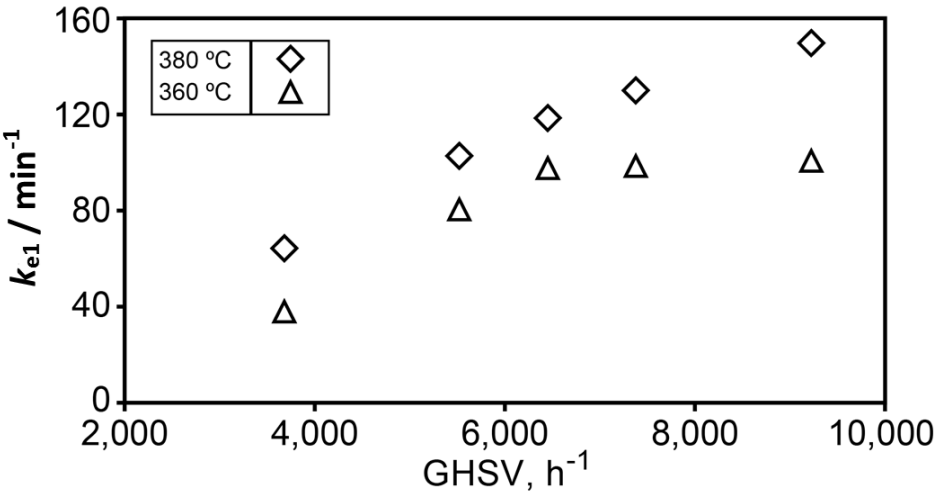

Figure 3.10: The dependence of effective rate constant (k_{e1}) on GHSV values for Zr-KIT-6 (20), p = 1 atm.

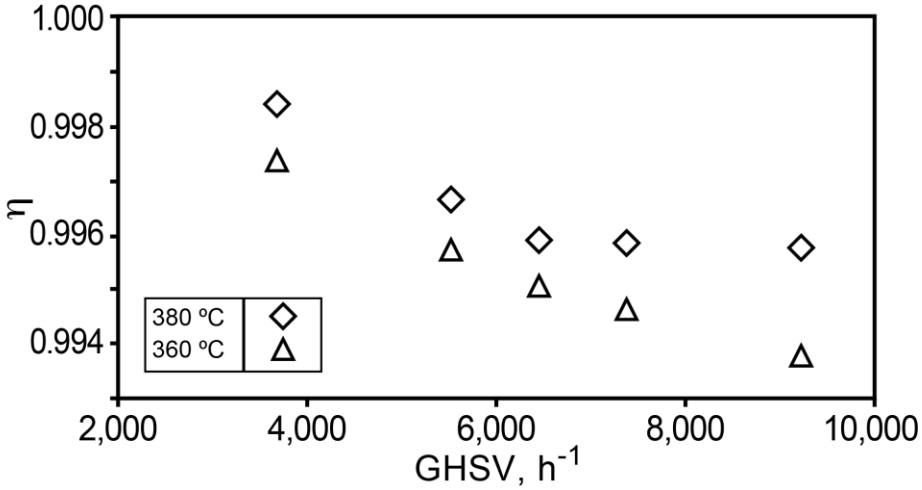

Figure 3.11 Estimation of internal effectiveness factors for EtOH dehydration over Zr-KIT-6 (20), p = 1 atm.

Estimation of Intrinsic Activation Energy for Ethanol Dehydration Reaction

The reaction was conducted at temperatures ranging from 300 to 360 °C, employing a GHSV of 7,200 h^{-1} in the absence of any mass transfer limitations for estimation of

activation energy. As shown in Figure 3.12a, the Zr-KIT-6 samples with higher Zr content yielded higher effective rate constants (k_{e1}) when such rate constants are normalized with respect to the volume of the catalyst packing (Eq. 3.7). The activation energy in each case was approximately 65-85 kJ/mol. When the rate constants were normalized with respect to the total acidity of the respective Zr-KIT-6 materials (Eq. 3.1), the rate constants at the various temperatures virtually overlapped for all the catalysts (Figure 3.12b). The intrinsic activation energy based on acidity-normalized rate constants was estimated to be approximately 79.5 ± 0.7 kJ/mol. Table 3.6 compares reported activation energies for catalytic dehydration of ethanol. The Zr-KIT-6 catalyst displays moderate activation energy.

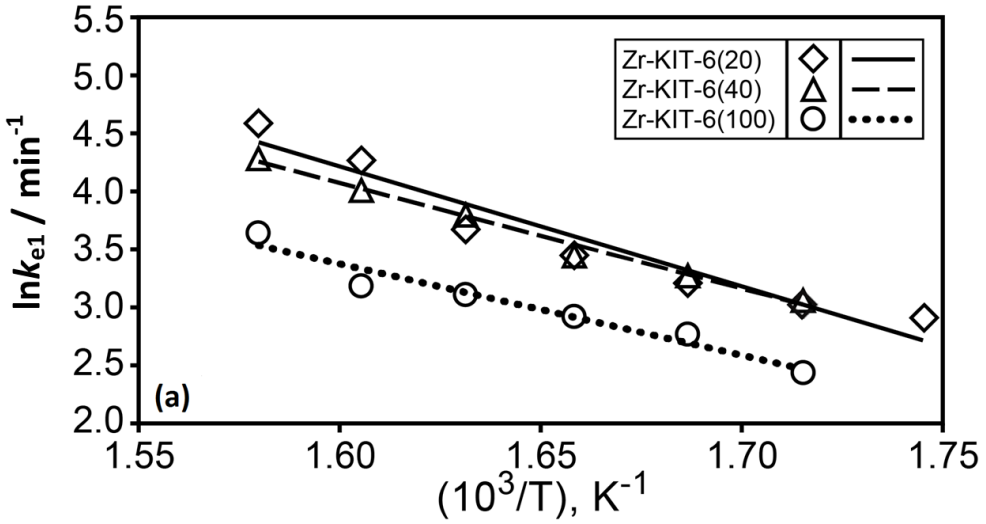

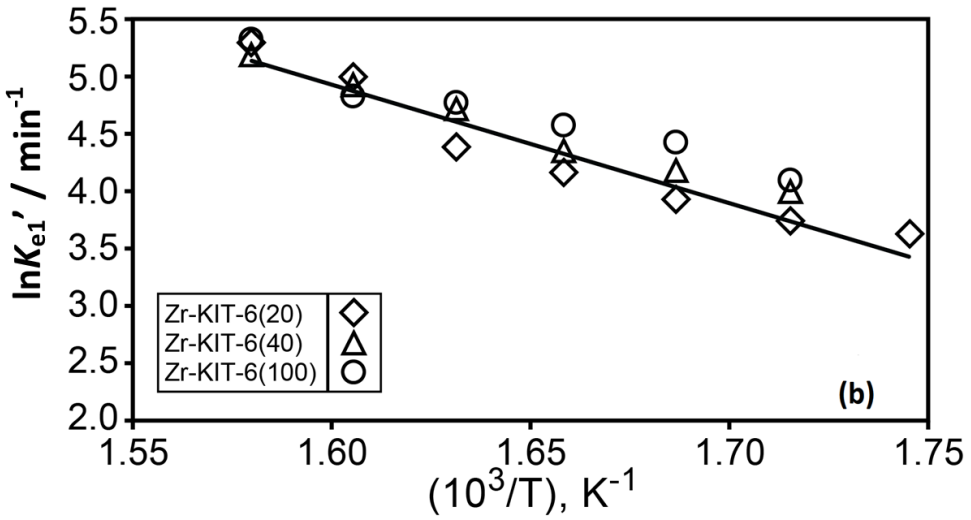

Figure 3.12: Estimation of activation energy of EtOH dehydration from (a) intrinsic rate constants (k_{e1}) based on catalyst packing volume, and (b) intrinsic rate constants (k_e') based on catalyst acidity.

Table 3.6: Comparison of activation energies for ethanol dehydration to ethylene over Zr-KIT-6 catalyst with those reported in the literature

Catalyst	**E (kJ/mol)**	**Reference**
Al_2O_3	53-78	[Bakoyannakis,2001]
Fe-ZSM-5	137.7	[Maihom, 2013]
Zr-KIT-6 (This work)	79.5	-

CHAPTER 4 CONCLUSIONS AND RECOMMENDATIONS

4.1 Conclusions

Zirconium incorporated mesoporous silicate, Zr-KIT-6, was evaluated for the dehydration of low alcohols, including isopropanol and ethanol. It was found that the predominantly Lewis acidity of the catalysts enhanced the yields of olefins.

For the dehydration of isopropanol to propene, high activity and selectivity (>98.5%) to propene were displayed in the 190-300°C temperature range. In sharp contrast, ZrO_2 displayed little acidity or dehydration activity, confirming the enhanced Lewis acidity of the Zr-KIT-6 materials. 12 and 30 hours continual run showed slight catalyst deactivation. First-order rate constant (k_e) based on a plug flow reactor model was applied for the kinetic study. Kinetic parameters obtained in the absence of external and internal mass transfer limitations showed moderate activation energy (~48.9 ± 0.5 kJ/mol) for all Zr-KIT-6 catalysts when normalized with the acid sites on the catalyst samples.

For the dehydration of ethanol to ethane, the observed ethanol conversions over the Zr-KIT-6 materials are similar to those for commercial ZrO_2, ranging from 15% -30% in the 300 - 360 °C range. However, the selectivity to ethylene (60- 80%) for Zr-KIT-6 materials was greater than that observed on commercial ZrO_2 powder (~40%). Catalyst stability testing on Zr-KIT- (100) showed deactivation starting at 70 hours. Taking account the parallel side reaction involving dehydrogenation to form diethyle ether, the intrinsic rate constants on all the catalysts overlap when normalized with the acid sites on

the catalyst samples. The corresponding intrinsic activation energy for ethanol dehydration to form ethylene was found to be 79.5 ± 0.7 kJ/mol.

The results presented in this work demonstrate that Zr-KIT-6 materials are superior Lewis acidic catalysts that display high activity, selectivity and durability that could be potentially exploited in the dehydration of various substrates. The emerging biomass-based renewable chemicals industry will particularly benefit from the availability of such catalysts for dehydration of long-chain alcohols from biomass based feedstock.

4.2 Recommendations

Based on the results from this thesis, future studies could focus on the following points:

1. Apply Zr-KIT-6 materials to the dehydration of longer chain alcohols to investigate the performance and stability of the catalyst for those reactions.
2. Develop microkinetic models to gain better fundamental insights into the underlying reaction mechanisms.
3. Investigate the mechanism of catalyst deactivation.
4. Investigate the application of Zr-KIT-6 to the dehydration of sugar alcohols (such as glycerol, sorbitol and xylitol) to valuable chemical intermediates.

REFERENCES

Bakoyannakis, D. N., D. Zamboulis, et al. The effect of preparation method on the catalytic acitivity of amorphous aluminas in ethanol dehydration. *Journal of Chemical Technology and Biotechnology*, 76:1159-1164, (2001).

Barbosa, L. A. M. M. and R. A. van Santen. Study of the Hydrolysis of acetonitrile using different Brøsted acid models: zeolite-type and $HCl(H_2O)_x$ clusters. *Journal of Catalysis*, 191: 200-217, (2000).

Barford, N. C. Experimental measurements: precision, error and truth. 2nd Ed. John Wiley & Sons, Inc., London, Great Britain. (1985)

Bokade, V. V., and Yadav, G. D. Heteropolyacid supported on montmorillonite catalyst for dehydration of dilute bio-ethanol. *Applied Clay Science*, 53(2): 263-271, (2011).

Bond, G. C., S. J.Frodsham, and P. Jubb, et al. Compensation effect in isopropanol dehydration over heteropoly acid catalysts at a gas-solid interface. *Journal of Catalysis* 293: 158-164, (2012).

Braskem Ethanol-to-Ethylene Plant, Brazil. (http://www.chemicals-technology.com/projects/braskem-ethanol/, accessed in July 2013).

Bravo-Suárez, J., R. V. Chaudhari, and B. Subramaniam. Design of heterogeneous catalysts for fuels and chemicals processing: an overview. In Novel Materials for Catalysis and Fuels Processing *ACS Symposium Series 1132*, Bravo-Suarez, Kidder, and Schwartz, Eds. 3-68, (2013).

Carmona, A.R., R. M. Tost, and J. M. Robles, et al. Preparation, characeterization and catalytic application of ZrO2 supported on low cost SBA-15. *Adsorption*, 17: 527-538, (2011).

Chemsystems, PERP Program - Alternative routes to propylene. (http://www.chemsystems.com/about/cs/news/items/PERP%200809S8_Propylene.cfm, accessed in July, 2013)

Chen, L. F., X. L. Zhou, and L. E. Norena, et al. Comparative studies of Zr-based MCM-41 and MCM-48 mesoporous molecular sives: synthesis and physicochmical properties. *Applied Surface Science*, 253: 2443-2451, (2006).

Chen, S. Y., J. F. Lee, and S. Cheng. Pinaco-type rearrangement catalyzed by Zr-incorporated SBA-15. *Journal of Catalysis*, 270: 196-205, (2010).

Chen, Y., Y. Wu, and L. Tao, et al. Dehydration reation of bio-ethanol to ethylene over modified SAPO catalysts. *Journal of Industrial & Engineering Chemistry*, 16: 717-722, (2010).

Crisci, A.J., M. H. Tucker, and M. Y. Lee, et al. Acid functionalized SBA-15-type silica catalysts for carbonhydrate dehydration. *ACS Catalysis*, 1: 719-728, (2011).

Cussler, E. L. Diffusion mass transfer in fluid systems. 2nd Ed. Cambridge University Press, NY, USA. (1997).

Doheim, M. M., and H. G. El-Shobaky. Catalytic conversion of ethanol and iso-propanol over ZnO-treated Co3O4/Al2O3 solids. *Colloids and Surfaces A: Physicochemical and Engineering Aspects*, 204: 169-174, (2002).

El Haskouri, J., S. Cabrera, and C. Guillem, et al. Atrane precursors in the one-pot surfactant-assisted synthesis of high zirconium content porous silicas. *Chemstry Materials*, 14: 5015-5022, (2002).

Fan, D., D. J. Dai, and H. S. Wu. Ethylene formation by catalytic dehydration of ethanol with industrial consderation. *Materials*, 6: 101-115, (2013).

Fuller, E. N., P. D. Schettler, J.C. Giddings. A new method for prediction of binary gas-phase diffusion coefficients. *Industrial and Engineering Chemistry*, 58(5): 18-27, (1966).

Guan, Y., Y. Li, and R. A. V. Santen. Controlling reaction pathways for alcohol dehydration and dehydrogenation over FeSBA-15 catalysts. *Catalysis Letters*, 117: 18-24, (2007).

Haishi, T., K. Kasai, and M. Iwamoto. Fast and quantitive dehydration of lower alcohols to corresponding olefins on mesoporous silica catalyst. *Chemistry Letter*, 40, (2011)

Herrera, J.E., J. H. Kwak, and J. Z. Hu, et al. Synthesis, characterization, and catalytic function of novel highly dispersed tungsten oxide catalysts on mesoporous silica. *Journal of Catalysis*, 239: 200-211, (2006).

Huber, G. W. and J. A. Dumesic. An overview of aqueous-phase catalytic processes for production of hydrogen and alkanes in a biorefinery. *Catalysis Today*, 111: 119-132, (2006a)

Huber, G. W., S. Iborra, and A. Corma. Synthesis of transportation fuels from biomass: chemistry, catalysts, and engineering. *Chemical Reviews*, 106: 4044-4098, (2006b)

Iglesias, J.; J. A. Melero; and L. F. Bautista, et al. Zr-SBA-15 as an efficient acid catalyst for FAME production from crude palm oil. *Catalysis Today*, 167: 46-55, (2011).

IHS (http://www.ihs.com/products/chemical/planning/ceh/propylene.aspx, accessed in July, 2013)

Jana, S.K., H. Takahashi, and M. Nakamura, et al. Aluminum incorporation in mesoporous MCM-41 molecular sieves and their catalytic performance in acid-catalyzed reactions. *Applied Catalysis A*: General, 245: 33-41, (2003).

Jiang, C., A. Su, and X. Li. Preparation of aluminosilicate mesoporous catalyst and its application for production 5-hydroxymethyl furfural dehydration from fructose. *Advanced Materials Research*, 392-398(2): 1190-1193, (2011).

Kalbasi, R.J. and N. Mosaddegh. Synthesis and characterization of Pd-poly(N-vinyl-2-pyrrolidone)/KIT-5 nanocomposite for heck reaction. *Materials Research Bulletin*, 47: 160-166, (2012).

Katiyar, A., S. Yadav, and P. G. Smirniotis, et al. Synthesis of ordered large pore SBA-15 spherical particles for adsorption of biomolecules. *Journal of Chromatography A*, 1122: 13-20, (2006).

Kim, T.W, R. Ryoo, and M. Kruk, et al. Tailoring the pore structure of SBA-16 silica molecular sieve through the use of copolymer blends and control of synthesis temperature and time. *Journal of Physical Chemistry B*, 108: 11480-11489, (2004).

Kleitz, F., D. Liu, and G. M. Anilkumar, et al. Large cage face-centered-cubic Fm3m mesoporous silica: synthesis and structure. *Journal of Physical Chemistry B*, 107: 14296-14300, (2003).

Kostova, N. G., A. A. Spojakina, and K. Jiratova. Hexagonol mesoporous silicas with and without Zr as supports for HDS catalysts. *Catalysis Today*, 65:217-223, (2001).

Kresge, C. T., M. E. Leonowicz, and W. J. Roth, et al. Ordered mesoporous molecular sieves synthesized by a liquid-crystal template mechanism. *Nature*, 359: 710-712, (1992).

Kruger, J. S., V. Nikolakis, and D. G. Vlachos. Carbohydrate dehydration using porous catalysts. *Current Opinion in Chemical Engineering*, 1: 312-320, (2012).

Kumaresan, L., A. Prabhu, and M. Palanichamy, et al. Mesoporous Ti-KIT-6 molecular sieves: Their catalytic activity in the epoxidation of cyclohexene. *Journal of the Taiwan Institute of Chemical Engineers*, 41(6): 670-675, (2010).

Laha, S.C., P. Mukherjee, and S.R. Sainkar, et al. Cerium containing MCM-41-type mesoporous materials and their acidic and redox catalytic properties. *Journal of Catalysis*, 207: 213-223, (2002).

Luz J., G.E., S. H. Lima, and A. C.R. Melo, et al. Direct synthesis and characeterization of LaSBA-15 mesoporous molecular sieves. *Journal of Material Science*, 45: 1117-1122, (2010).

Maihom, T., P. Khongpracha, and J. Sirjaraensre, et al. Mechanistic studies on the transformation of ethanol into ethane over Fe-ZSM-5 zeolite. *ChemPhysChem*, 14: 101-107, (2013).

Mazaheri, H., K. T. Lee, et al. Subcritical water liquefaction of oil palm fruit press fiber for the production of bio-oil: effect of catalysts. *Bioresource Technology*, 101: 745-751, (2010).

McNair, H. M. and J. M. Miller. Basic gas chromatography. New York, Wiley, (1998)

Mokaya, R. Improving the stability of mesoporous MCM-41 silica via thicker more highly condensed pore walls. *Journal of Physical Chemistry B*, 103: 10204-10208, (1999).

Naik, S.P., V. Bui, and T. Ryu, et al. Al-MCM-41 as methanol dehydration catalyst. *Applied Catalysis A*: General, 381: 183-190, (2010).

Okajima, I. and T. Sako. Energy conversion of biomass with supercritical and subcritical water using large-scale plants. *Journal of Bioscience and Bioengineering*, (2013) in press.

Paris, C., M. Moliner, and A. Corma, Metal-containing zeolites as efficient catalysts for the transformation of highly valuable chiral biomass-derived products. *Green Chemistry*, 15: 2101-2109, (2013).

Pavia, D. L., G. M. Lampman, et al. Introduction to organic laboratory techniques (4th Ed.). 797–817, (2006)

Phillips, C. B. and R. Datta. Production of ethylene from hydrous ethanol on H-ZSM-5 under mild Conditions. *Industrial & Engineering Chemistry Research*, 36: 4466-4475, (1997)

Prabhu, A., L. Kumaresan, and M. Palanichamy, et al. Synthesis and characterization ofn aluminium incorporated mesoporous KIT-6: Efficient catalyst for acylation of phenol. *Applied Catalysis, A: General*, 360(1): 59-65, (2009).

Prabhu, A., A. A. Shoaibi, and C. Srinivasakannan, et al. Prominent catalytic activity of mesoporous molecular sieves in the vapor phase dehydration of cyclohexanol to cyclohexene. *Journal of Rare Earths*, 31 (5): 477-484, (2013).

Prestianni, A., R. Cortese, and D. Duca. Propan-2-ol dehydration on H-ZSM-5 and H-Y zeolite: a DFT study. *Reaction Kinetics Mechanisms and Catalysts*, 108: 565-582, (2013)

Ramanathan, A., B. Subramaniam, R. Maheswari, et al. Synthesis and characterization of zirconium incorporated ultra large pore mesoporous silicate, Zr-KIT-6. *Microporous and Mesoporous Materials*, 167: 207-212, (2013).

Rakshe, B., V. Ramaswamy, and A. V. Ramaswamy. Acidity and m-xylene isomerization activity of large pore, zirconium-containing alumino-silicate with BEA structure. *Journal of Catalysis*, 188: 252-260, (1999).

Rouquerol, J., D. Avnir, and C. W. Fairbridge, et al. Recommendations for the characterization of porous solids. *Pure and Applied Chemistry*, 66 (8): 1739-1758, (1994).

Rüfer, A., A. Werner, and W. Reschetilowski. A study on the bifunctional isomerization of n-decane using a superior combination of design of experiments and kinetic modeling. *Chemical Engineering Science*, 87: 160-172, (2013).

Saxena, R. C., D. K. Adhikari, and H. B. Goyal. Biomass-based energy fuel through biochemical routes: A review. *Renewable and sustainable energy reviews*, 13: 167-178, (2009)

Song, Z., W. Liu, and C. Chen, et al. Production of propylene from ethanol over ZSM-5 co-modified with zirconium and phosphorus. *Reaction Kinetics Mechanisms and Catalysis*, 109: 21-231 (2013).

Takahara, I., M. Saito, and M. Inaba, et al. Dehydration of ethanol into ethylene over solid acid catalysts. *Catalysis Letters*, 105 (3): 249-252, (2005)

Takahara, I., M. Saito, and H. Matsuhashi, et al. Increase in the number of acid sites of a H-ZSM-5 zeolite during the dehydration of ethanol. *Catalysis Letters*, 113 (3): 82-85, (2007)

Thorat, I. V., D. E. Stephenson, N. A. Zacharias, et al. Quantifying tortuosity in porous Li-ion battery materials. *Journal of Power Sources*, 188: 592-600, (2009).

Turek, D., J. Haber, et al. Dehydration of isopropyl alcohol used as an indicator of the type and strength of catalyst acid centres. *Applied Surface Science*, 252: 823-827, (2005)

Verma, S. R. and P. R. Chqudhari. Limnological studies on Indian brackish water lonar lake with special reference to trophic status and potential public utility. *Industrial & Engineering Chemistry Research*, 17(4): 49-58 (2013).

Vijayalaxmi, S., K. A. A. Appaiah, et al. Production of bioethanol from fermented sugars of sugarcane bagasse produced by lignocellulolytic enzymes of exiguobacterium sp. VSG-1. *Applied Biochemistry and Biotechnology*, (2013) in press.

Visuvamithiran, P., M. Palanichamy, and K. Shanthi, et al. Selective epoxidation of olefins over Co(II)-Schiff base immobilized on KIT-6. *Applied Catalysis, A: General*, 462: 31-38, (2013).

West, R. M., Braden, D. J., and Dumesic, J. A. Dehydration of butanol to butene over solid acid catalysts in high water environments. *Journal of Catalysis*, 262(1): 134-143, (2009).

Wu, L., X. Shi, and Q. Cui, et al. Effects of the SAPO-11 synthetic process on dehydration of ethanol to ethylene. *Frontiers of Chemical Science & Engineering*, 5: 60-66, (2011).

Zhang M. and Y. Yu. Dehydration of ethanol to ethlene. *Industrial & Engineering Chemistry Research*, 52:9505-9514, (2013)

Zhang, X., R. Wang, and X. Yang, et al. Comparison of four catalysts in the catalytic dehydration of ethanol to ethylene. *Micaroporous and Mesoporous Materials*, 116: 210-215, (2008).

APPENDIX A ERROR ANALYSIS AND CALIBRATIONS

A.1 Causes of Experimental Error

Experimental error is the difference between a measured value of quantity and its true value. There are two main types of experimental error: systematic errors and random errors [Barford, 1985].

Systematic errors arise from faults or changes in conditions which are often constant and could be corrected or allowed for. In this study, systematic errors were reduced by properly calibrating the measuring instruments such as balance, thermocouples and mass flow controller.

Random errors are caused by intrinsic and unpredictable fluctuations in the apparatus. These errors can be properly characterized by repeated measurements.

A.2 Mean and Standard Deviation

In order to minimize and quantify the error, mean and standard deviation were applied to the experimental data analysis [Barford, 1985]. Mean (X_n) is the best estimate of the true value from repeated measurements (Eq. A.1). Standard deviation (S_n) shows how much variation or dispersion exists from the mean (Eq. A.2). The results of an experiment (X) may be summarized in the form of Eq. A.3.

$$X_n = \sum_i x_i / n \qquad \text{(Eq. A.1)}$$

$$S_n{}^2 = \frac{\sum_i (x_i - X_n)}{n-1} \qquad \text{(Eq. A.2)}$$

$$X = X_n \pm S_n \quad \text{(Eq. A.3)}$$

Where, Xi = measured values

n = number of measurements

A.3 Correlation

An important aspect of experimental research concerns the question of whether the observations provide good evidence for a relationship between two measured quantities. For example, both the concentration and peak area of a substance are measured values for GC calibration, and the response factor correlating both is to be addressed. To solve this problem, linear regression was applied (Eq. A.4) [Barford, 1985].

$$y_i = \hat{y}_i + E_i$$

$$\hat{y}_i = ax_i + b \quad \text{(Eq. 2.5)}$$

Where, y_i = measured value of y

x_i = measured value of x

$\hat{y}_i$ = value of y predicted by regression

a = estimate of the slope of the regression line

b = estimate of the intercept of the regression line

E_i = model error

In Eq. A.4, Assuming x_i have negligible errors, the errors in a and b arise only from errors in y_i. As for the GC calibration, the concentration of a substance was

regarded as the precise value (x_i), and the peak area was regarded as the dependent variable (y_i).

The expressions for slope (a), intercept (b) and standard deviation for slope was obtained as follows [Barford, 1985]:

$$a = \frac{n\sum xy - \sum x \sum y}{n\sum x^2 - (\sum x)^2} \quad \text{(Eq. A.5)}$$

$$b = \frac{\sum x^2 \sum y - \sum x \sum xy}{n\sum x^2 - (\sum x)^2} \quad \text{(Eq. A.6)}$$

$$S_n(a) = \frac{n\sigma(y)(\sum(x^2)^{\frac{1}{2}}}{\{n(n-2)[n\sum x^2 - (\sum x)^2]\}^{\frac{1}{2}}} \quad \text{(Eq. A.7)}$$

Where, $\sigma(y) = \sqrt{\overline{y^2} - (\bar{y})^2}$

The degree of correlation is evaluated by the coefficient of correlation R (Eq. A.8). The value of R varies in the range of -1 to 1. The greater the value of R, the greater the justification for believing that the two measured quantities are really linked or correlated. For a perfect correlation, R = ±1; if there is no correlation, R=0.

$$R = \frac{n\sum xy - \sum x \sum y}{[n\sum x^2 - (\sum x)^2]^{\frac{1}{2}}[n\sum y^2 - (\sum y)^2]^{\frac{1}{2}}} \quad \text{(Eq. A.8)}$$

The GC calibration curves and error analysis are provided below.

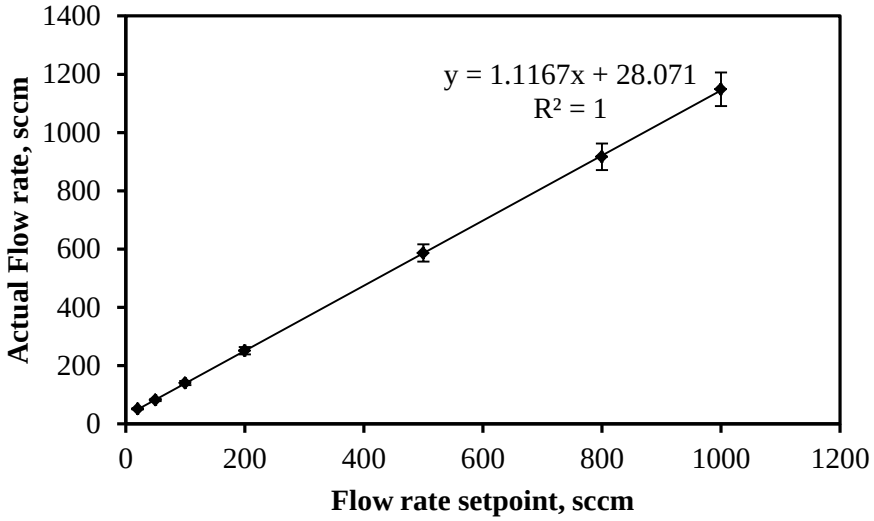

Figure A.1: Mass flow controller calibration curve

Table A.1: Mass flow controller calibration curve data

Flow rate set point, mL/min	Average actual flow rate standard cm^3/min	standard deviation
20	52	0.00
50	82	0.94
100	140	0.47
200	252	1.25
500	587	0.47
800	917	1.25
1000	1148	0.94

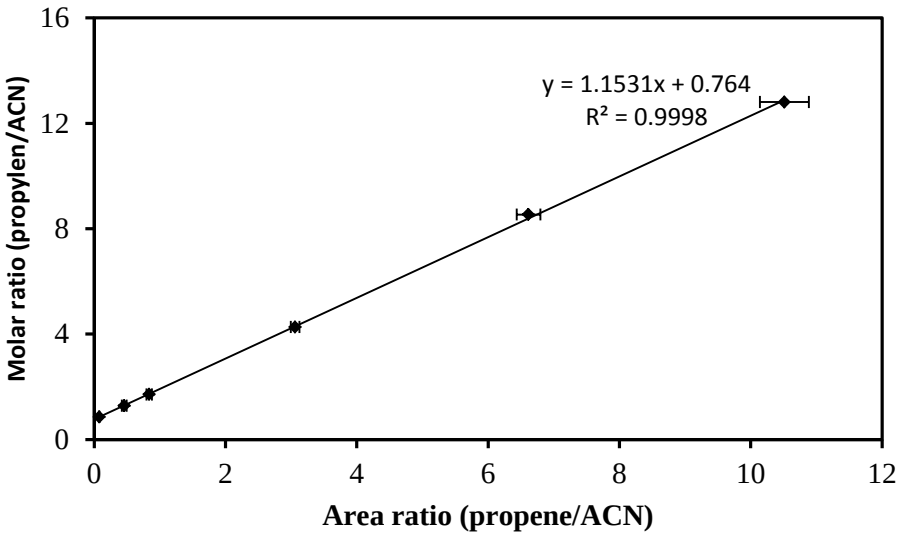

Figure A.2: Propene calibration curve

Table A.2: Propene calibration curve data

Molar ratio (propene/ACN)	Average area ratio (propene/ACN)	standard deviation
0.8538	0.0791	0.0036
1.2807	0.4599	0.0360
1.7076	0.8382	0.0435
4.2691	3.0622	0.0663
8.5381	6.6165	0.1782
12.8072	10.5146	0.3737

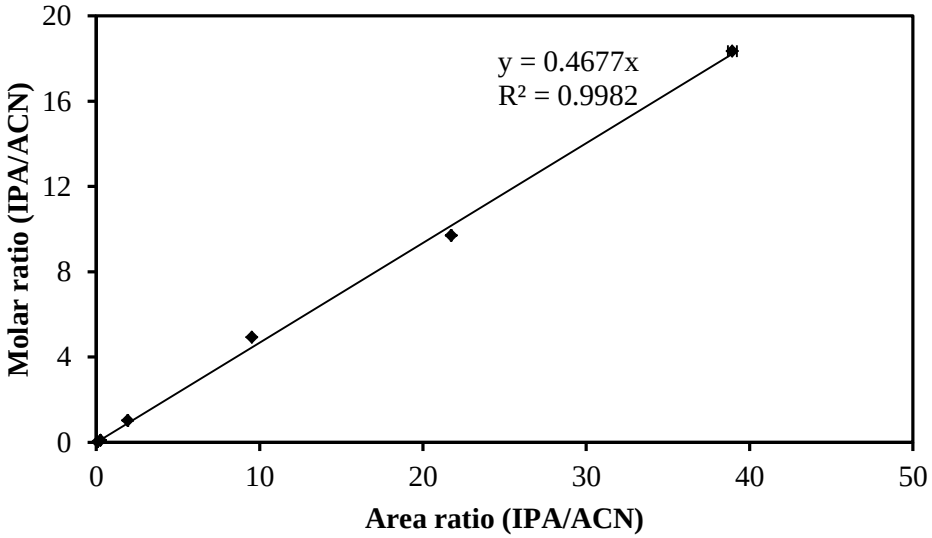

Figure A.3: Isopropanol calibration curve

Table A.3: Isopropanol calibration curve data

Molar ratio (IPA/ACN)	Average area ratio (IPA/ACN)	standard deviation
0.0205	0.0766	0.0012
0.1015	0.2558	0.0005
1.0227	1.9346	0.01134
4.9302	9.5297	0.0011
9.7083	21.7399	0.0271
18.3510	38.9429	0.2811

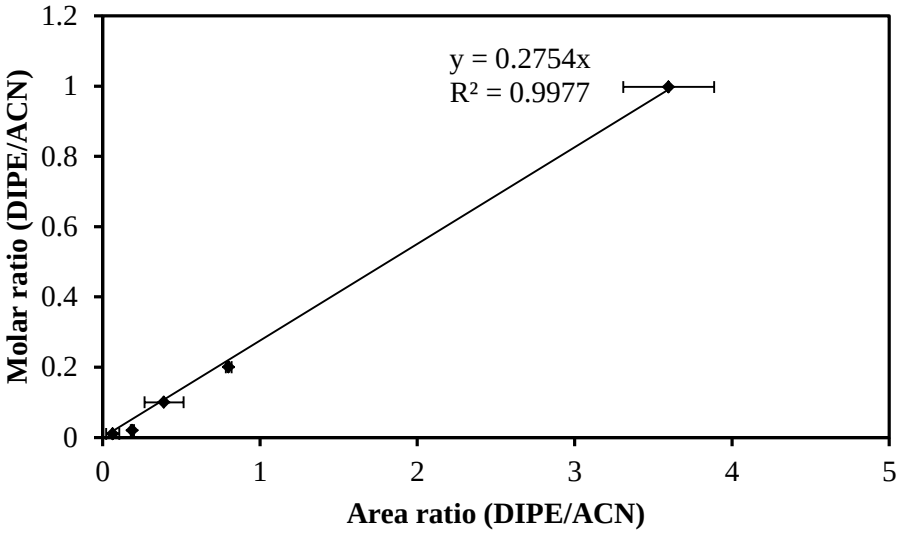

Figure A.4 Diisopropyl ether calibration curve

Table A.4 Diisopropyl ether calibration curve data

Molar ratio (DIIE/ACN)	Average area ratio (DIIE/ACN)	standard deviation
0.9978	3.5974	0.2884
0.2000	0.8010	0.0189
0.1001	0.3903	0.1234
0.0204	0.1882	0.0101
0.0102	0.0639	0.0423

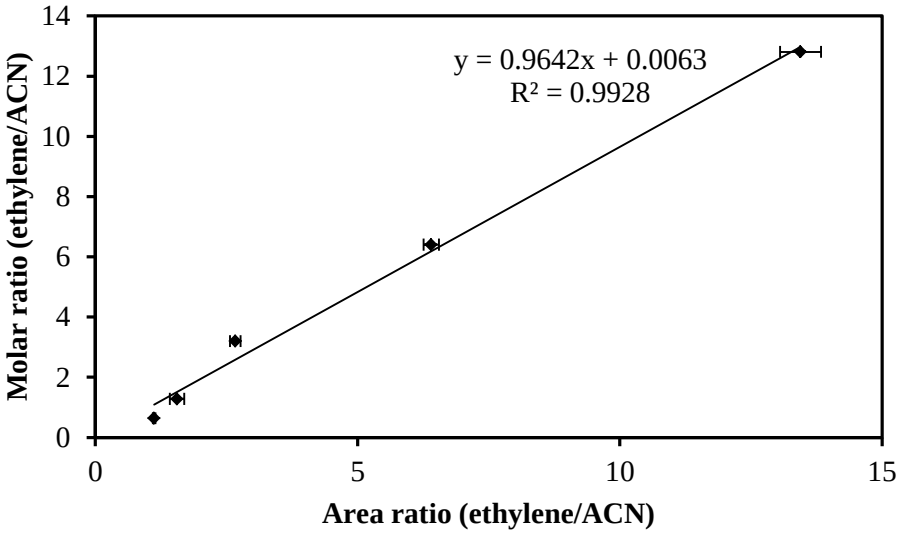

Figure A.5: Ethylene calibration curve

Table A.5: Ethylene calibration curve data

Molar ratio (Ethylene/ACN)	Average area ratio (Ethylene/ACN)	standard deviation
0.6404	1.216	0.0271
1.2808	1.5600	0.1382
3.2018	2.6708	0.1013
6.4036	6.4044	0.1453
12.8072	13.4467	0.3925

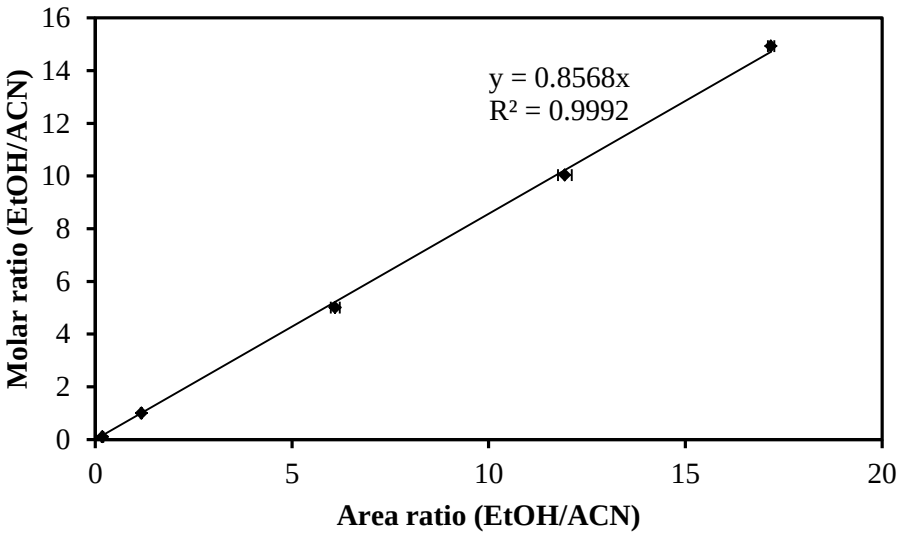

Figure A.6: Ethanol calibration curve

Table A.6: Ethanol calibration curve data

Molar ratio (EtOH/ACN)	Average area ratio (EtOH/ACN)	standard deviation
0.1000	0.1814	0.0240
0.9990	1.1725	0.0197
5.0068	6.0989	0.1146
10.0355	11.9367	0.1721
14.9305	17.1799	0.0802

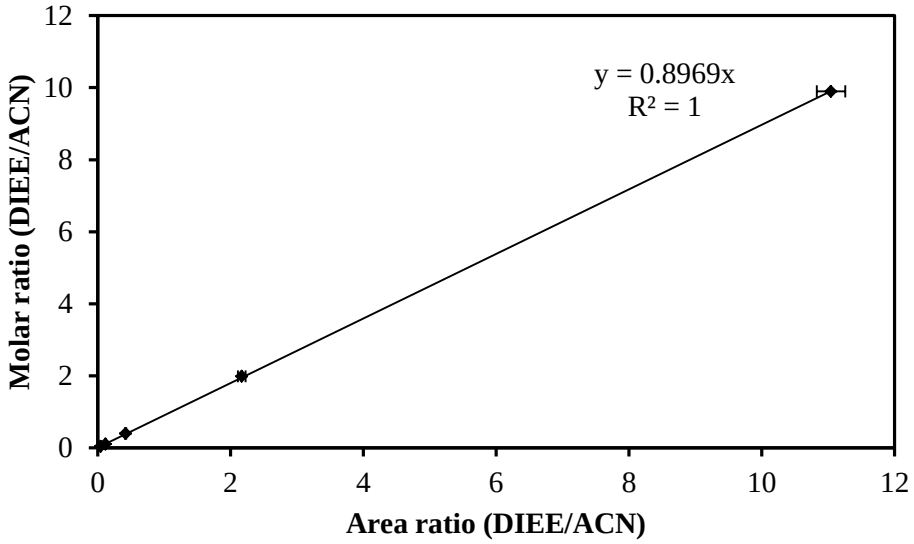

Figure A.7: Diethyl ether calibration curve

Table A.7: Diethyl ether calibration curve data

Molar ratio (DIEE/ACN)	Average area ratio (DIEE/ACN)	standard deviation
0.0403	0.0453	0.0006
0.1032	0.1179	0.0031
0.3974	0.4210	0.0097
1.9836	2.1703	0.0566
9.8968	11.0429	0.2135

APPENDIX B Calculation of the Effectiveness Factor

The bulk diffusion coefficient for IPA diffusing in N_2 was evaluated by Fuller's correlation (Eq. B.3) [Fuller, 1966]. And the effective coefficient of IPA and N_2 transport in pore was calculated by Eq. B.4 [Cussler 2nd Ed. 1997]. The tortuosity is estimated by Bruggeman relationship (Eq. B.6) [Thorat, 2009]. The equations are listed as follows.

$$\eta = \frac{3}{\varphi^2}(\varphi coth\ \varphi - 1) \quad \text{(Eq. B.1)}$$

$$\varphi = \sqrt{k_e R^2 / D_e} \quad \text{(Eq. B.2)}$$

$$D_{AB} = \frac{1.00\times10^{-3} T^{1.75} \left(\frac{1}{M_A}+\frac{1}{M_B}\right)^{1/2}}{p\left[\left(\sum_A \vartheta_i\right)^{1/3}+\left(\sum_B \vartheta_i\right)^{1/3}\right]^2} \quad \text{(Eq. B.3)}$$

$$D_e = \frac{\varepsilon D_{AB}}{\tau} \quad \text{(Eq. B.4)}$$

$$\varepsilon = 1 - \frac{\rho_b}{\rho_p} \quad \text{(Eq. B.5)}$$

$$\tau = \varepsilon^{1-m} \quad \text{(Eq. B.6)}$$

Where, φ =Thiele modulus

k_e = intrinsic rate constant (s^{-1})

R = radius of catalyst pellet (m)

D_e = effective diffusion coefficient (m^2/s)

D_{AB} = binary diffusion coefficient for IPA diffusion in N_2 (m^2/s)

T = temperature (K)

M_A, M_B = molecular weights of IPA (A) and N_2 (B) (g/mol)

p = reactor pressure (atm)

ϑ_i = special diffusion parameters over the atoms of the diffusing species

$\emptyset$ = porosity of the catalyst

τ = tortuosity

ρ_b = bulk density of the catalyst

ρ_p = particle density of the catalyst

m = Bruggeman exponent (1.6)

Table B.1: Detailed calibration data of effectiveness factor for IPA dehydration

Cat. Sample	GHSV	k_e (min^{-1})	φ	η
Zr-KIT-6 (20)	2400	220.01	0.1133	0.9991
	4800	400.23	0.1528	0.9984
	6000	700.02	0.2020	0.9973
	7200	712.07	0.2037	0.9972
	9600	760	0.2105	0.9971
	12000	759.12	0.2104	0.9971
Zr-KIT-6 (40)	2400	141.59	0.0909	0.9995
	4800	293.78	0.1309	0.9989
	6000	398.78	0.1525	0.9985
	7200	402.69	0.1532	0.9984
	9600	403.17	0.1533	0.9984
	12000	405.08	0.1537	0.9984
Zr-KIT-6 (100)	2400	59.9	0.0591	0.9998
	4800	113.59	0.0814	0.9996
	6000	291.12	0.1303	0.9989
	7200	292.98	0.1307	0.9989
	9600	293.01	0.1307	0.9989
	12000	292.77	0.1306	0.9989

Parameters: T= 533.2K, ϑ_H=2.31, ϑ_C=15.9, ϑ_O=6.11, ϑ_N=4.54, τ=1, ρ_b=375 kg/m^3, ρ_p=1000 kg/m^3, R= 237.5 µm, D_{AB}=3.5×10^{-5} m^2/S, D_e=2.2×10^{-5} m^2/S, ε=0.625, τ=1.36.